Active faulting in the Walker Lane

Steven G. Wesnousky

Center for Neotectonic Studies, University of Nevada, Reno, Nevada, USA

Received 2 March 2004; revised 15 December 2004; accepted 3 February 2005; published 16 June 2005.

[1] Deformation across the San Andreas and Walker Lane fault systems accounts for most relative Pacific–North American transform plate motion. The Walker Lane is composed of discontinuous sets of right-slip faults that are located to the east and strike approximately parallel to the San Andreas fault system. Mapping of active faults in the central Walker Lane shows that right-lateral shear is locally accommodated by rotation of crustal blocks bounded by steep-dipping east striking left-slip faults. The left slip and clockwise rotation of crustal blocks bounded by the east striking faults has produced major basins in the area, including Rattlesnake and Garfield flats; Teels, Columbus and Rhodes salt marshes; and Queen Valley. The Benton Springs and Petrified Springs faults are the major northwest striking structures currently accommodating transform motion in the central Walker Lane. Right-lateral offsets of late Pleistocene surfaces along the two faults point to slip rates of at least 1 mm/yr. The northern limit of northwest trending strike-slip faults in the central Walker Lane is abrupt and reflects transfer of strike-slip to dip-slip deformation in the western Basin and Range and transformation of right slip into rotation of crustal blocks to the north. The transfer of strike slip in the central Walker Lane to dip slip in the western Basin and Range correlates to a northward broadening of the modern strain field suggested by geodesy and appears to be a long-lived feature of the deformation field. The complexity of faulting and apparent rotation of crustal blocks within the Walker Lane is consistent with the concept of a partially detached and elastic-brittle crust that is being transported on a continuously deforming layer below. The regional pattern of faulting within the Walker Lane is more complex than observed along the San Andreas fault system to the west. The difference is attributed to the relatively less cumulative slip that has occurred across the Walker Lane and that oblique components of displacement are of opposite sense along the Walker Lane (extension) and San Andreas (contraction), respectively. Despite the gross differences in fault pattern, the Walker Lane and San Andreas also share similarities in deformation style, including clockwise rotations of crustal blocks leading to development of structural basins and the partitioning of oblique components of slip onto subparallel strike-slip and dip-slip faults.
Citation: Wesnousky, S. G. (2005), Active faulting in the Walker Lane, *Tectonics*, *24*, TC3009, doi:10.1029/2004TC001645.

0278-7407/05/2004TC001645$12.00

1. Introduction

[2] Pacific–North American relative plate motion at the latitude of the San Andreas fault system is ~50 mm/yr (Figure 1) [*DeMets and Dixon*, 1999]. The transform motion is taken up largely along the San Andreas fault system. Up to one fourth of the strike-slip motion is distributed on faults east of the San Andreas fault system within the Eastern California Shear Zone and the Walker Lane [*Bennett et al.*, 1998, 2003; *Dixon et al.*, 1995; *Dokka and Travis*, 1990a, 1990b; *Minster and Jordan*, 1987; *Oldow et al.*, 1994; *Reheis and Dixon*, 1996; *Sauber*, 1994; *Sauber et al.*, 1986; *Thatcher et al.*, 1999]. I present here the results of a field study of a set of active faults in the central Walker Lane (Figure 1). The area encompasses a right step in the northwest trending system of strike-slip faults. The purpose of the study is to lend clarity to the style, recency of displacement, and slip rate of active faults in the area. The resulting observations provide the underpinnings of discussion bearing on the role of active faulting in the structural and physiographic development of the region, mechanisms of displacement transfer along the discontinuous set of faults defining the Walker Lane, the relationship of active faults to variations in measures of geodetic strain along the Walker Lane, and reasons for similarities and differences in styles of faulting between the Walker Lane and San Andreas fault systems. For context, I first review available observations describing strain accumulation and the history of slip on faults within the Eastern California Shear Zone and Walker Lane. The results of the field study are provided in the subsequent observations section.

2. The Eastern California Shear Zone and Walker Lane: Displacement History and Strain Accumulation

2.1. Overview

[3] The term Eastern California Shear Zone (ECSZ) was first used by *Dokka and Travis* [1990b] for the set of northwest striking right-lateral faults that cut the Mojave Desert (Figure 1). The earliest accounts of strike-slip faulting east of the Sierra Nevada include *Gianella and*

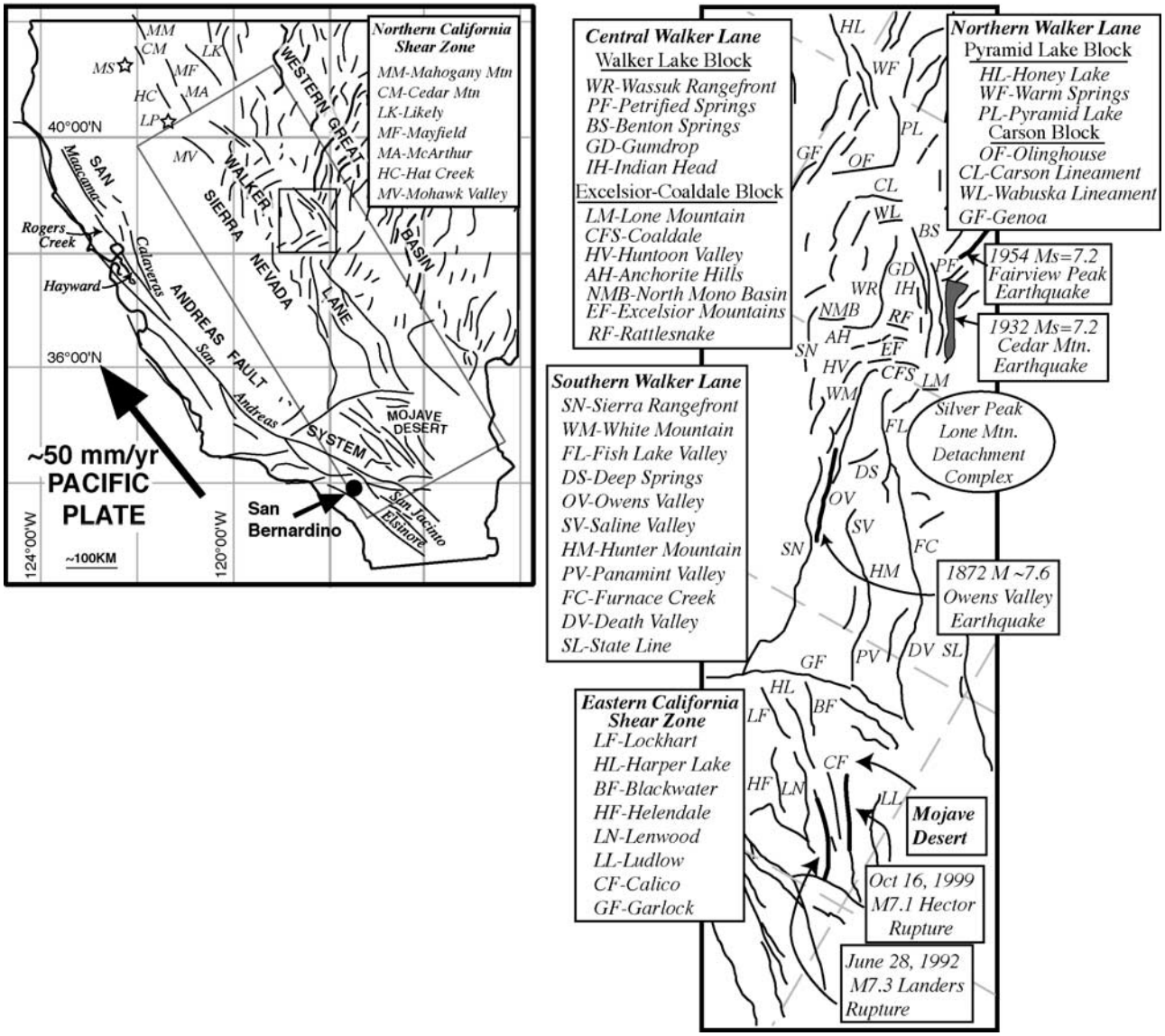

Figure 1. (left) Regional fault map. The Walker Lane and Eastern California Shear Zone are outlined by large box. (right) Larger scale map. Small box on left bounds faults mapped in this study. Fault names are annotated and regions subdivided for convenience of discussion. Locations of 26 March 1872 *M*7.6 Owens Valley, 28 June 1992 *M*7.3 Landers, and 16 October 1999 *M*7.1 Hector surface ruptures are denoted by thicker lines. Area enveloping 1932 M_s7.2 Cedar Mountain earthquake ground ruptures is shaded gray. Mount Shasta (MS) and Lassen Peak are shown by stars. Pacific–North American relative plate motion vector is from the work of *DeMets and Dixon* [1999].

Callaghan's [1934] description of the 1932 Cedar Mountain earthquake and the mapping of *Ferguson and Muller* [1949] and *Nielsen* [1965]. The zone of strike-slip faults and associated disrupted topography, all or in part, has been referred to as the Walker Lane [*Locke et al.*, 1940], the Walker Line [*Billingsley and Locke*, 1941], the Walker Belt [*Stewart*, 1980], and the Walker Lane Belt [*Carr*, 1984]. For convenience, I use the term Walker Lane to encompass the zone of right-lateral faults that extends northward from the Garlock fault. *Stewart* [1980] brought to attention that the pattern of faulting in the Walker Lane is structurally complex and does not consist of a single throughgoing system of right-lateral faults. He divided the Walker Lane into 9 discrete ''structural blocks.'' The grouping and labeling of Walker Lane fault domains in Figure 1 is modified from his work.

2.2. The Eastern California Shear Zone of the Mojave Desert

[4] The San Andreas fault bends sharply westward at the latitude of San Bernardino where it forms the southwest

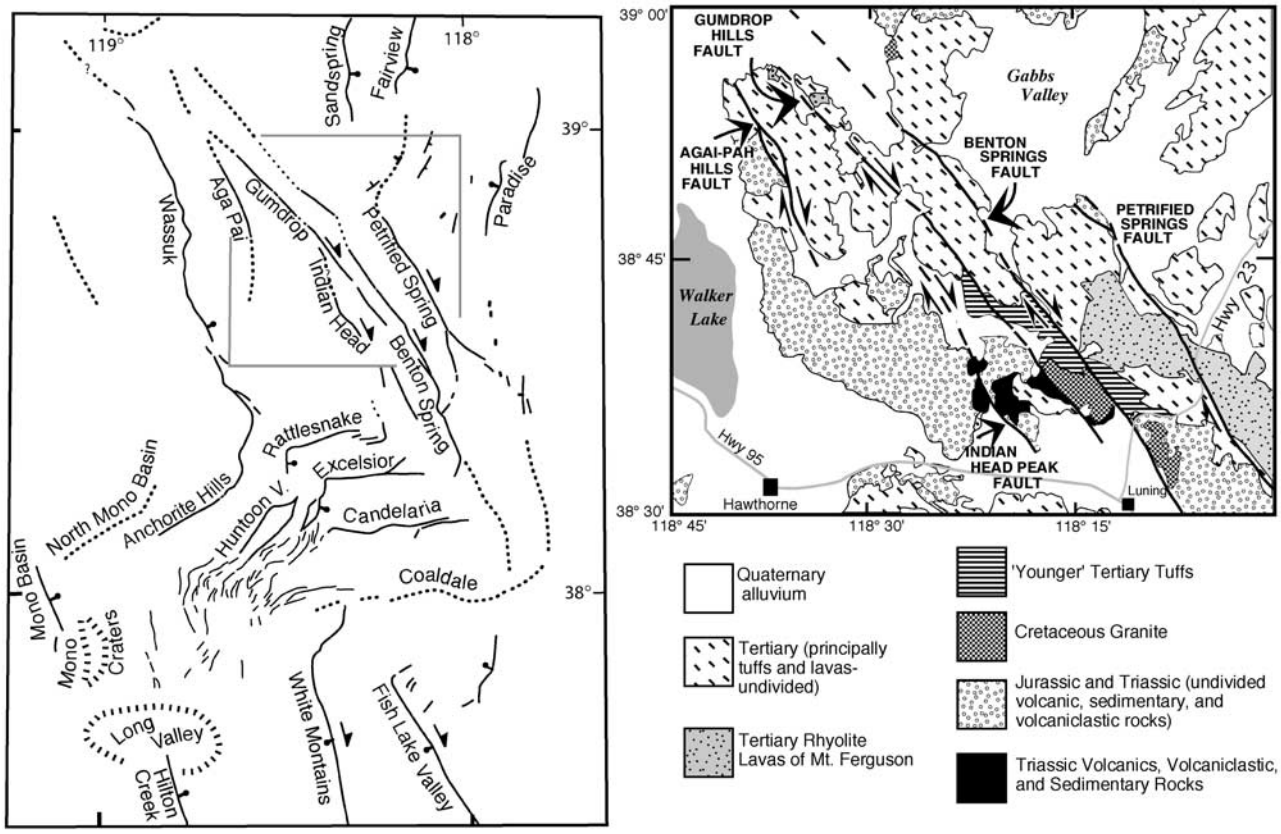

Figure 2. (left) Map of active faults in and around central Walker Lane. (right) Map of northwestern trending faults of central Walker Lane and dextrally offset Tertiary and older rocks. Location is shown by small box at left (simplified from work of *Ekren and Byers* [1984]). Half-sided arrows show sense of strike slip.

margin of the Mojave Desert (Figure 1). There the right-lateral shear deformation associated with the Pacific–North American plate boundary is partially transferred from the San Andreas to a broadly distributed and complex shear zone that extends northwestward through the Mojave and then further northward through the Walker Lane. The Eastern California Shear Zone consists of at least seven major faults, each of which shows a steep dip, right slip, and anastomosing and en echelon fault segments. *Dokka* [1983] and *Dokka and Travis* [1990a] report 65–80 km of right-lateral offset of Miocene terrain across the faults. They further interpret that displacement commenced between 10 and 6 Ma (perhaps as recently as 1.5 to 0.7 Ma) and that the cumulative slip represents at least 9–14% of Pacific–North American plate motion during that time. The 28 June 1992 Landers (M_w 7.3) and 16 October 1999 Hector Mine (M_w 7.1) earthquakes occurred on faults within this zone. *Sauber* [1994] analyzed a geodetic network spanning the Eastern California Shear Zone and the northern portion of the Landers earthquake rupture. The analysis shows the equivalent of ~12 mm/yr of right-lateral slip across the region, approximately 25% of the total North American–Pacific plate motion budget. The east striking left-lateral Garlock fault does not now appear to be accumulating left-lateral simple shear strain due to slip at depth [*Savage et al.*, 2001], despite geologic evidence for both long-term and Holocene left-lateral slip [*Davis and Burchfiel*, 1973; *McGill and Rockwell*, 1998; *Smith*, 1962]. Geodetic measurements show right-lateral strain accumulation within the Eastern California Shear Zone is continuous across the Garlock fault into the southern Walker Lane [*Peltzer et al.*, 2001; *Savage et al.*, 2001]. The curvature of the Garlock fault may be the result of the accumulation of strain within the Mojave [*Dokka and Travis*, 1990a]. The bending may provide a mechanism to transmit strain, and thus stress, northward.

2.3. The Southern Walker Lane

[5] The southern Walker Lane extends northward from the Garlock fault. Major northwest striking right-lateral strike-slip fault systems include the Owens Valley fault, the Panamint Valley–Hunter Mountain–Saline Valley fault system, and the Death Valley–Furnace Creek–Fish Lake Valley fault system.

[6] Estimates of total right slip on the Furnace Creek–Fish Lake Valley fault zone range from 40–100 km based on offsets of various stratigraphic and geochemical markers and isopach trends [*Stewart*, 1988]. *Reheis and Sawyer* [1997] favor a value of 40–50 km arising from *McKee*'s [1968] observation of an offset Jurassic quartz monzonite in

Table 1. Radiocarbon Samples

Sample	Lab Numbers CAMS[a]	^{14}C Age[b] ± 2σ	δ^{13}C[c]	Calendar Age,[d] years B.P. ± 2σ
T5-C	98693	1415 ± 45	−25	1335 ± 70
BT1-1RC	100582	2940 ± 35	−20.5	3088 ± 122
BT1-5ARC	100969	780 ± 35	−22.1	709 ± 49
NCRC-SGW	100580	3960 ± 35	−22.1	4407 ± 115

[a]Center for Accelerator Mass Spectrometry (CAMS) at Lawrence Livermore National Laboratory.
[b]Uses Libby's half-life 5568 years.
[c]The δ^{13}C values without decimal places are the assumed values according to *Stuiver and Polach* [1977]. Values with a single decimal place are measured for the material itself.
[d]Dendrochronologically calibrated ages calculated with Web-based University of Washington Calibration Program [*Stuiver and Reimer*, 1993].

northern Death Valley. Displacement initiated between 12 and 8 Ma [*Reheis and McKee*, 1991; *Reheis and Sawyer*, 1997; *Stewart*, 1988]. Paleozoic rocks are right laterally offset 16–19 km along the State Line fault to the east [*Stewart*, 1988]. Right-lateral displacement on the Hunter Mountain fault is on the order of 8–10 km in the last 4 Myr [*Burchfiel et al.*, 1987]. Net right slip on the Owens Valley Fault has been considered to be no more than a few kilometers [*Moore and Hopson*, 1961; *Ross*, 1962] though *Beanland and Clark* [1994] suggest that 10–20 km of right slip is permissive. *Kylander-Clark et al.* [2005] and J. M. Bartley et al. (Large dextral offset across Owens Valley, California, and its possible relation to tectonic uproofing of the southern Sierra Nevada, submitted to *Special Paper of the Geological Society of America*, 2005) recognize 65 ± 5 km of right slip across Owens Valley since 83.5 Ma, but also point to regional relationships to interpret that most of the displacement took place in latest Cretaceous–early Tertiary, prior to development of the San Andreas transform fault system. Thus net right slip across the region since inception of the San Andreas transform is no more than ∼150 km and by favored estimates less than ∼100 km. Within attendant uncertainties, the timing and cumulative amount of right slip registered across the southern Walker Lane is similar to or slightly greater than observed across the Eastern California Shear Zone.

[7] Slip rates based on geology have been reported for the major strike-slip faults. Dextral slip along the northern Death Valley fault zone is 3–9 mm/yr near Red Wall Canyon [*Klinger*, 2001]. *Reheis and Dixon* [1996] observe the slip rate to increase northward by ∼3–5 mm/yr on the northern Furnace Creek and Fish Lake Valley fault zones, respectively, though average rates along the Fish Lake Valley fault zone are dependent on the location and the time spanned by the measurement [*Reheis and Sawyer*, 1997]. The suggested increase corresponds to the fault intersection with northeastern trending normal faults of Eureka Valley and Deep Springs Valley, and probably relates to a transfer of slip eastward from the Hunter Mountain–Saline and White–Inyo fault systems along northeast striking normal faults in Deep Springs and Eureka Valleys [*Lee et al.*, 2001a; *Oswald and Wesnousky*, 2002; *Reheis and Dixon*, 1996]. *Zhang et al.* [1990] interpret Holocene dextral slip at 2.4 ± 0.8 mm/yr on the southern Panamint Valley fault zone. Geomorphic and

Table 2. Tephra Samples

Sample	Lab Numbers[a]	Age[a]	Name
081899-T3	4605/T438-8	∼1–2 ^{14}C ka	Mono[b]
SGW-C9	4986/T492-1	<2.56 to 2.81 Ma	lower tuffs of the Badlands at Willow Wash[c]
		<3.5 < 4.2 Ma	or Tuff of Curry Canyon[c]
SGW-HE17	4987/T492-2	<2.56–2.81 Ma	Lower tuffs of the Badlands at Willow Wash[c]
SGW-HW21	4988/T492-3	.9–1.0 ^{14}C ka	Mono[b]
SGW-HW13[d]		.9–1.0 ^{14}C ka	Mono[b]
TA1a	4989/T492-4	3.4 Ma	Putah Tuff[c]
SGW-BT1-ASH1	5183/T508-2	0.8–1.2 ^{14}C ka	Mono[b]
SGW-BT1-ASH2	5184/T508-3	3.3–3.9 ^{14}C ka	Mono[b]
NCT1-SGW	5185/T508-4	0.8–1.2 ^{14}C ka	Mono[b]

[a]Correlation and age estimates were provided by A. M. Sarna-Wojcicki (Head), E. Wan (Lab Supervisor), J. Walker (electron microprobe analyst), and M. Dodge and K. Hepper (Physical Science Technicians) at the Tephrochronology Laboratory at USGS in Menlo Park using a JEOL 8900 Superprobe. The method of analysis is described by *Sarna-Wojcicki and Davis* [1991].
[b]Corresponding ages of Mono ashes are based on best correlation to tephra layers previously dated by ^{14}C but do not exclude the possibility that the tephra may be as young as ∼600 or as old as ∼6700 years, a period over which numerous compositionally very similar tephras were ejected from the Mono Craters area.
[c]Refer to *Sarna-Wojcicki et al.* [2005] for type localities.
[d]Correlation by author is based on proximity and identical stratigraphic setting to sample SGW-H21.

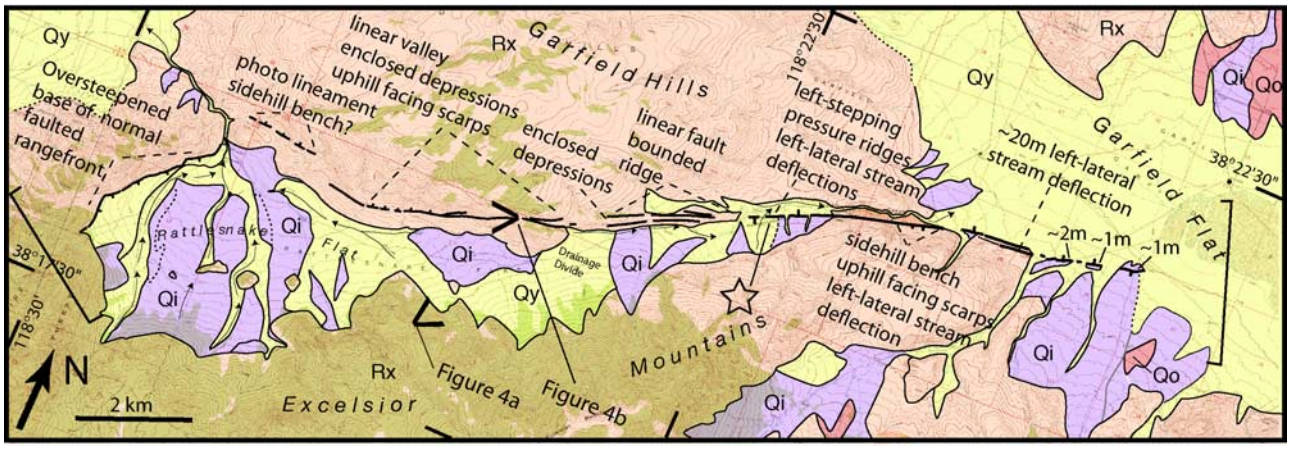

Figure 3. Rattlesnake fault trace and distribution of Quaternary deposits. Scarp heights and features indicative of sense of offset and ongoing fault activity are annotated. Units Qy, Qi, and Qo are Quaternary deposits of relatively increasing age (see text for discussion). Unit Rx is undifferentiated bedrock. Faults (bold lines) are dashed and dotted where approximately located or inferred, respectively. Direction of view for photos in Figure 4 is indicated by open end of solid bold rotated V shapes. Topographic map is provided in Figure 5 of site marked by star.

climatic considerations suggest a 3.3–4.0 mm/yr right-lateral slip rate along the Hunter Mountain fault zone over the last 15 thousand years [*Oswald and Wesnousky*, 2002]. Right lateral slip during the Holocene has averaged between 1 and 4 mm/yr along the Owens Valley fault [*Beanland and Clark*, 1994; *Lee et al.*, 2001b; *Lubetkin*, 1988]. The 1872 M_w 7.6 Owens Valley earthquake produced dextral offsets averaging about 6 m along the ~100 km fault length [*Beanland and Clark*, 1994]. Normal and right-slip components of slip on the White Mountains frontal fault has averaged ~0.1 mm/yr [*dePolo*, 1989] and 0.3 ± 0.2 mm/yr, respectively [*Reheis and Dixon*, 1996]. Estimates of the normal displacement rate of the Sierra Nevada frontal fault adjacent to the Owens Valley fault range between 0.1 and 0.2 mm/yr [*Gillespie*, 1982; *Reheis and Dixon*, 1996].

[8] Space geodetic data show >10 mm/yr of north-northwest directed right-lateral shear is being accommodated across the southern Walker Lane [*Dixon et al.*, 1995; *Gan et al.*, 2000]. The value is similar to the rates observed to the south in the Eastern California Shear Zone. *Reheis and Dixon* [1996] reproduce the observed strain field across the area with a fault model that assumes right-lateral slip at depth on the individual fault systems: Owens Valley fault zone, 3.9 ± 1.1 mm/yr; Death Valley–Furnace Creek fault zone, 3.3 ± 2.2 mm/yr; White Mountains fault zone in northern Owens Valley, 3.4 ± 1.2 mm/yr; and Fish Lake Valley fault zone, 6.2 ± 2.3 mm/yr. Analysis of a linear array of monuments across the region by *Gan et al.* [2000] yields slightly different results: Owens Valley fault, 6.9 ± 1.6 mm/yr; Death Valley Furnace Creek, 3.2 ± 0.9 mm/yr; and Hunter Mountain–Panamint Valley fault, 3.3 ± 1.6 mm/yr. Both models show some inconsistency with available geologic observations. For example, the model of *Reheis and Dixon* [1996] requires a higher slip rate than is observed on the White Mountains fault zone. The *Gan et al.* [2000] model requires more slip be placed on the Owens Valley fault than is observed. It is not clear whether the inconsistencies are a reflection of the different time periods measured, viscoelastic response of the crust and upper mantle to historical earthquakes, or inadequacies of the geologic data.

2.4. The Central Walker Lane

[9] The region includes faults of *Stewart*'s [1988] Excelsior-Coaldale and Walker Lake blocks (Figures 1 and 2). Faults of the Excelsior-Coaldale Block generally strike east-northeast and display evidence of late Quaternary displacement [*dePolo*, 1993; *Oldow et al.*, 1994; *Stewart*, 1988; *Wetterauer*, 1977]. The east-northeast striking faults include the Candelaria, Excelsior Mountain, Huntoon Valley, Anchorite Hills, North Mono Basin, and Rattlesnake fault zones (Figure 2). The faults generally sit within a right step between northwest striking strike-slip faults of the southern Walker Lane and the Walker Lane Block to the north. The main strike-slip faults of the Walker Lane Block are, from east to west, the Petrified Springs, Benton Springs, Gumdrop Hills, and Indian Head Peak fault zones. The Walker Lane Block is bounded on the west by the east dipping active normal fault that bounds the east flank of the Wassuk Mountains. Offset Tertiary tuffs and lavas and older granites and volcaniclastic rocks are interpreted to indicate that the northwest striking strike-slip faults of the Walker Lane Block have taken up 48–60 km of right-lateral strike slip during the last 10–15 Myr [*Ekren and Byers*, 1984, 1985a, 1985b, 1986a, 1986b; *Ferguson and Muller*, 1949; *Hardyman*, 1980, 1984; *Hardyman and Oldow*, 1991; *Nielsen*, 1965]. The observations are consistent with the idea that slip from the southern Walker Lane is transferred to the Walker Lake Block via the Excelsior-Coaldale Block

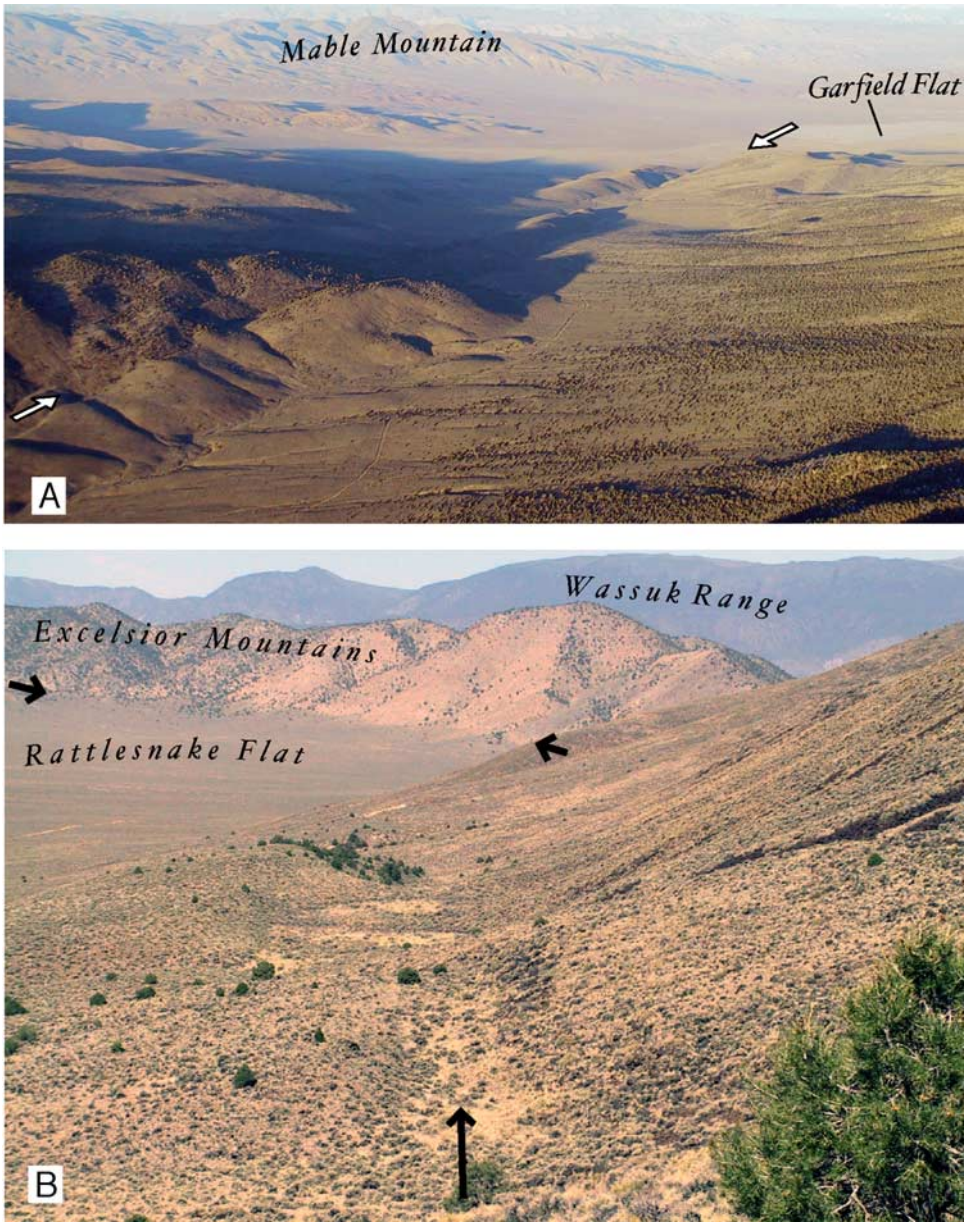

Figure 4. Rattlesnake fault. (a) View northwestward showing linear valleys and ridges, side hill benches, closed depressions, and uphill-facing scarps, which define the strike of Rattlesnake fault (along strike between arrows). View is to the northeast. (b) View westward along strike shows trace characterized by side hill bench and enclosed depression in foreground characteristic of strike-slip displacement. Trace bends sharply to south in distance and exhibits oversteepening of the range front and triangular facets indicating primarily normal fault displacement. Perspective of photos is shown on map in Figure 3.

[*Oldow*, 1992]. Geodetic observations indicate that the amount of right-lateral shear strain currently being accommodated within the central Walker Lane is about 10 mm/yr [*Bennett et al.*, 2003; *Oldow et al.*, 2001], similar to that observed to the south in the Eastern California Shear Zone and southern Walker Lane. Quaternary expression of faults within this region and the manner in which strain is accommodated by faults within the central Walker Lane is examined in detail later as a main focus of this paper.

[10] The M_w 7.2 Cedar Mountain earthquake of 1932 occurred immediately east of the Benton and Petrified Springs faults (Figure 1). The earthquake produced a discontinuous system of surface faults, fissures, and fractures encompassing a zone 10 km wide by about 70 km long and trending N20°E, more northerly than the strike-

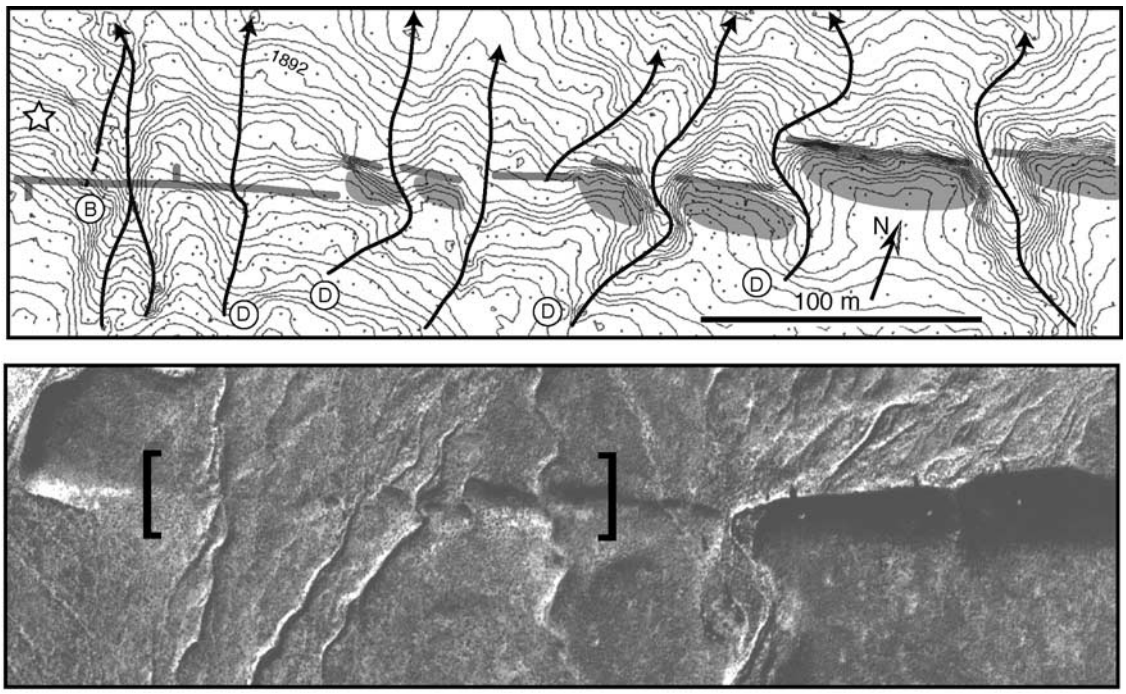

Figure 5. (bottom) Air photo and (top) topographic map along section of Rattlesnake fault. Topographic map covers region within brackets on air photo. Youthful offset has produced left stepping en echelon pressure ridges (shaded), left-lateral deflection of ephemeral stream channels (D), and a beheaded channel offset left laterally about 12 m (B). Contour interval is 0.35 m. Control points for contour map are dots. UTM coordinate of star on topographic map is NAD27 CONUS N4244343 E379928. Location is also marked by star on map in Figure 3.

slip faults of the Walker Lane Block [*Bell et al.*, 1999; *Caskey et al.*, 1996; *Gianella and Callaghan*, 1934]. The focal mechanism of the event shows right slip on a nodal plane also striking more northerly than the faults of the Walker Lake Block [*Doser*, 1988]. The right-lateral Holocene slip rate of the Cedar Mountain fault zone is estimated at between 0.2 and 0.7 mm/yr [*Bell et al.*, 1999]. The more northeasterly striking strands of the

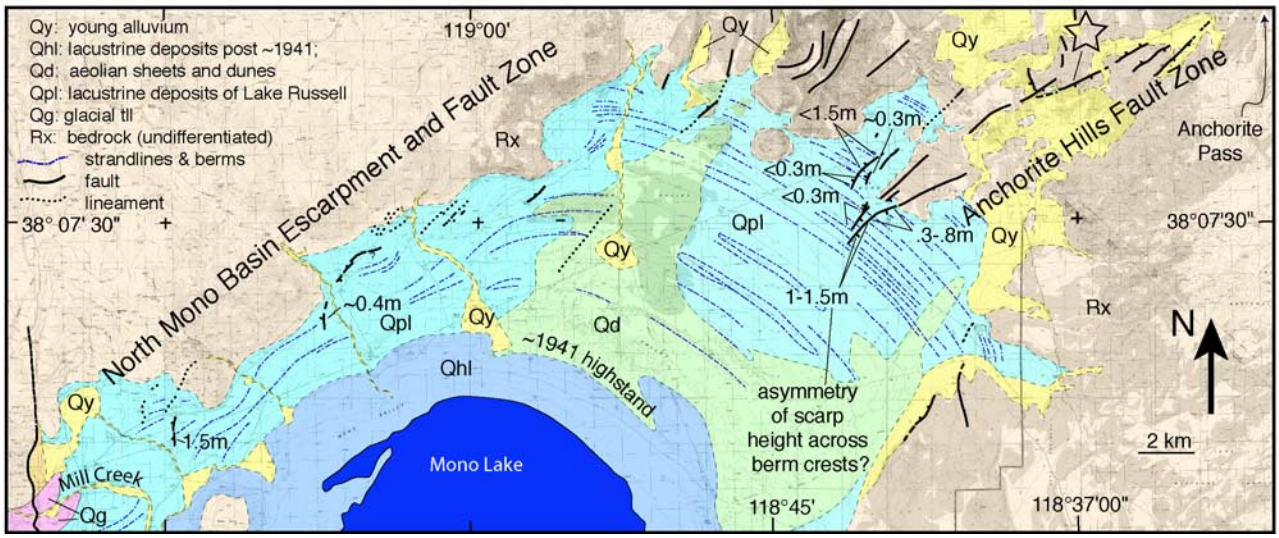

Figure 6. Map showing Anchorite Hills fault zone and scarps along the North Mono Basin escarpment. Scarp heights are annotated. Location of *Gilbert et al.*'s [1968] ~300 m left-lateral offset of 2.5 Ma bedrock is marked by star.

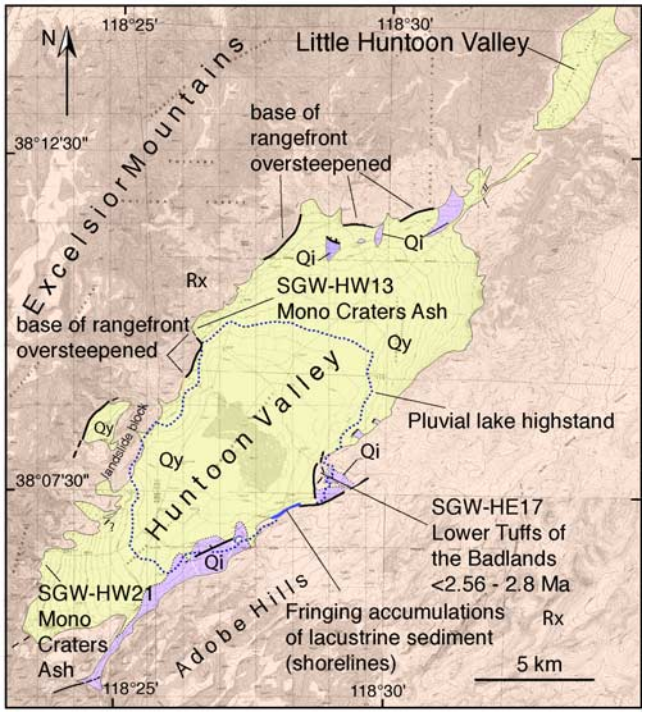

Figure 7. Map of Huntoon Valley annotated to show faults (bold lines), fault features, and distribution of Quaternary deposits. Units Qy and Qi are Quaternary deposits of relatively increasing age (see text for discussion). Coordinates (UTM NAD 27 CONUS) of tephra ash sample sites are SGW-HW13 (363305 4225113) and SGW-HW21 (359144 4218731).

surface rupture display primarily normal displacement [*Bell et al.*, 1999], and they overlap and strike parallel to surface ruptures of the 1954 Fairview Peak earthquake [*Caskey et al.*, 1996].

2.5. Northern Walker Lane

[11] This region encompasses the Carson and Pyramid Lake blocks of *Stewart* [1988]. The Carson Block is defined by northeast trending faults or lineaments of known or presumed left-lateral strike slip [*Ekren et al.*, 1976; *Rogers*, 1975; *Stewart*, 1988]. The Olinghouse fault and Wabuska Lineament mark the northern and southern bounds of the domain, and the Carson Lineament resides between (Figure 1). Holocene geomorphic features are offset left laterally along the Olinghouse fault [*Sanders and Slemmons*, 1979, 1996]. *Briggs and Wesnousky* [2001] document two large earthquakes on this fault during the last ~3500 years. It is suggested, though not accepted with unanimity, that a magnitude 6.7 event occurred along the fault in 1869 [*Sanders and Slemmons*, 1979, 1996; *Toppozada et al.*, 1981]. The Carson Lineament is a structural zone expressed by near alignment of valleys and mountain ranges and numerous northeast striking faults [*Rogers*, 1975; *Stewart*, 1988]. The Carson and Wabuska lineaments have been considered, though never clearly documented, to be left slip based on a trend parallel to the Olinghouse fault [*Bell*, 1984; *Rogers*, 1975; *Slemmons et al.*, 1979; *Stewart*, 1988]. Miocene basalts in the Carson Block are reported to show 37° to 51° of clockwise vertical axis rotation since 9–13 Ma [*Cashman and Fontaine*, 2000]. Northwest oriented right-lateral displacement through this region may be accomplished by clockwise rotation of crustal blocks bounded by deep-seated, high-angle, northeast striking left-lateral strike-slip faults such as the Olinghouse fault [*Cashman and Fontaine*, 2000]. The Carson Block is bounded to the west by active normal faults that trend northerly and delineate the western extent of Basin and Range extension (Figure 1). *Ramelli et al.* [1999] report Holocene normal displacement on the Genoa fault is 2–3 mm/yr. Similar information appears lacking for other normal faults in this region.

[12] The Pyramid Lake Block encloses a set of left stepping northwest trending active strike-slip faults that, from south to north, include the Pyramid Lake, Warm Springs Valley, and Honey Lake faults (Figure 1). The Mohawk Valley fault shares a similar strike, sits farther to the west within the Sierra Nevada, and is also probably right-lateral strike slip. At least three surface rupture events have occurred on the Pyramid Lake fault since ~7500 years B.P. [*Anderson and Hawkins*, 1984]. Offset geomorphic features indicate the Holocene slip rate of the Pyramid Lake fault is at minimum ~1 mm/yr and probably >3 mm/yr [*Briggs and Wesnousky*, 2004]. Right-lateral offset and natural exposure on an incised creek channel are interpreted by *Wills and Borchardt* [1993] to indicate four or more Holocene surface rupture earthquakes and a slip rate of 1.1–2.6 mm/yr for the Honey Lake fault zone. Similar studies are lacking for the other major strike-slip faults. Rates of geodetically observed strain accumulation across the northern Walker Lane are less than observed to the south. *Thatcher et al.* [1999] estimate 6 ± 2 mm/yr is concentrated across the zone. The difference of this value with respect to the greater rates observed to the south is distributed on normal faults to the west in the western Basin and Range [*Bennett et al.*, 2003; *Thatcher et al.*, 1999].

2.6. Northern California Shear Zone

[13] A northern California shear zone is defined here by a number of similarly northwest oriented faults that cut Quaternary rocks and are evident on the map of *Jennings* [1994]. The faults include the Mahogany Mountain, Cedar Mountain, Mayfield, McArthur, Hat Creek, and Mohawk Valley fault zones (Figure 1). The zone remains poorly defined and little studied. The Mohawk Valley fault zone is associated with a distributed zone of seismicity that extends northward into Mounts Lassen and Shasta of the Cascade Volcanic arc [*Goter et al.*, 1994].

3. Observations: Active Faults of the Central Walker Lane

[14] The primary observations of the field study are provided here. The methods and basis of description are outlined first. Description of the individual faults follows. The order of description is geographic. Descriptions of east

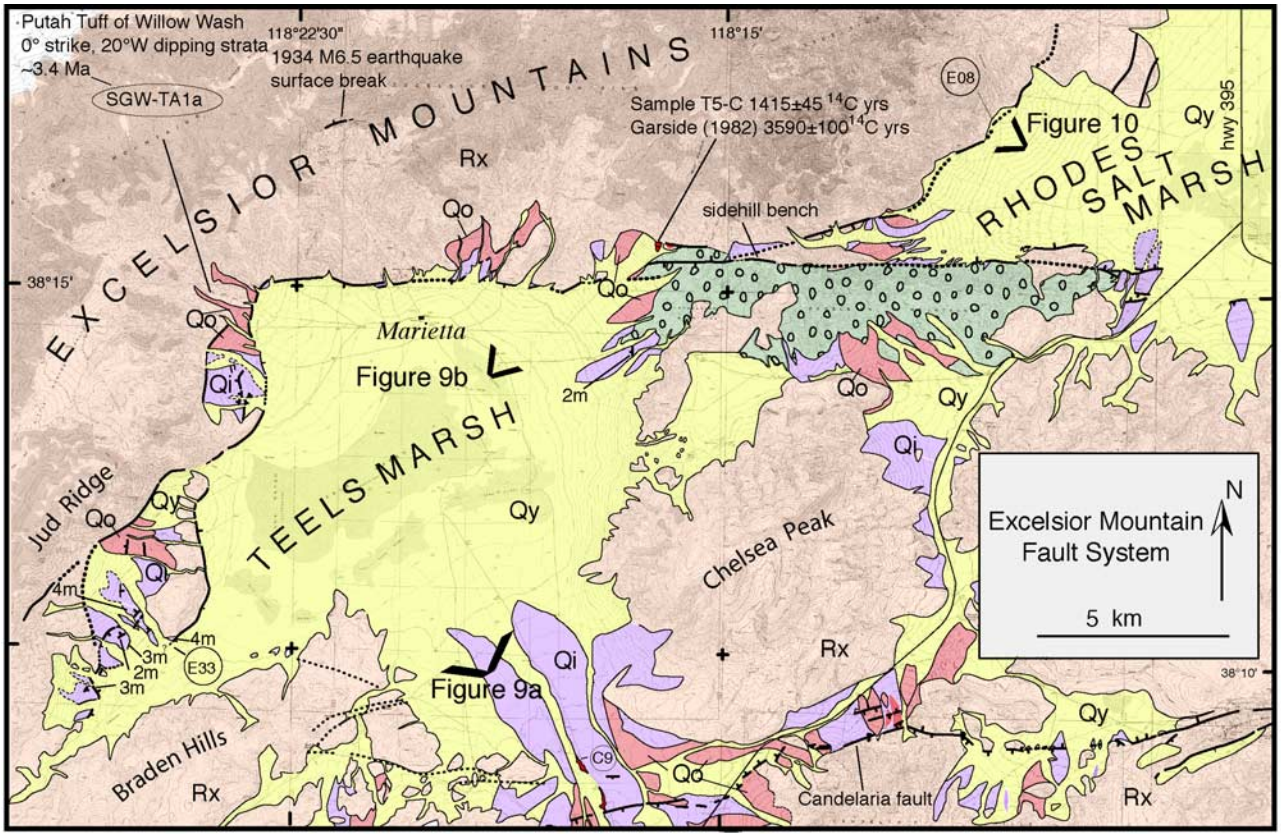

Figure 8. Excelsior Mountain fault traces. Scarp heights and features indicative of sense of offset and ongoing fault activity are annotated. Units Qy, Qi, and Qo are Quaternary deposits of relatively increasing age (see text for discussion). Unit Rx encompasses primarily undifferentiated bedrock. Stippled area is Tertiary gravel. Perspective of photos in Figure 9 and 10 is indicated by open end of bold rotated V shapes.

striking faults of the system are initially described and ordered from north to south. The major northwest striking faults are then considered from east to west. The observations most salient to the discussion that follows are gathered in a synopsis at the end of this section.

3.1. Methods

[15] Fault descriptions are based on field observations aided by examination of large-scale (~1:12,000) conventional black and white aerial photography collected along each of the fault zones. My primary purpose is to document features bearing on the recency and kinematics of Quaternary movement along each fault and, where observations allow, the timing of past earthquakes and average rates of fault displacement. The observations are largely synthesized on a set of maps. The maps show active fault traces and are annotated to indicate the location of features indicative of the sense, style and amount of offset of geomorphic features. Active lateral slip along strike-slip faults results in a distinct set of geomorphic features including enclosed depressions, shutter ridges, medial ridges, offset and deflected streams, linear side hill benches, uphill facing scarps, aligned notches and spurs, and fault-controlled drainages. Normal faults commonly bound mountain fronts that, depending on the degree of fault activity, display triangular facets, "wineglass" canyons, and a more sinuous and disrupted trace than strike-slip fault traces. Diagrams and discussion of the morphology developed along strike slip and normal faults are given by *Vedder and Wallace* [1970] and *Wallace* [1978a, 1990].

[16] The fault trace maps also show at a reconnaissance level the distribution of Quaternary deposits in the vicinity of each fault. For each fault area, I generally limit the subdivision of Quaternary deposits to 3 units based principally on variation in surficial characteristics including degree of dissection, elevation above modern stream grade, and tonal and textural differences on air photos. The basis of the approach is described by *Bull* [1991] and the maps of *Dohrenwend* [1982a, 1982b] and *Reheis et al.* [1995] are applications of the method. Here, the oldest Quaternary deposits (Qo) are considered to be mid-Pleistocene to late Pleistocene in age. They are characterized by deeply dissected fan remnants commonly showing rounded or sharp crests that are on the order of 10 m or more above modern stream grade, and are separated from younger depositional surfaces by erosional scarps. Depositional surfaces interpreted to be of intermediate age (Qi) generally rest no more

Figure 9. (a) View to northwest across Teels Marsh and Excelsior Mountains. Truncated and uplifted fan surfaces, triangular facets, and oversteepening at the base of the range front show faulting to be active along the south and southeastern front of the Excelsior Mountains. The fault trace strikes northward from the left foreground to near the center of the photo at which point it bends sharply ~90° and strikes east. (b) Linear trace (arrows), reversal of scarp facing directions, and narrow along-strike valley in the pass between Teels and Rhodes salt marshes marking the Excelsior Mountains Fault as it extends eastward (right) out of the view toward Pilot Mountains. Perspective of photos is annotated in Figure 8.

than about 10 m above modern grade, exhibit lesser amounts of dissection, are more often characterized by relatively broader, smooth, and flat interfluvial fan remnants, and generally here considered to be late Pleistocene in age. The youngest fan deposits (Qy) include undissected active fan and wash surfaces that exhibit levee and channel or fresh bar and swale topography and few if any well defined postabandonment drainage channels. The divisions are broad, likely overlap between fault areas, and do not provide a chronosequence. Rather, they serve to provide the reader additional context to observe and interpret the distribution of fault related morphology that I report along each of the fault zones. Mapping of young deposits along each of the faults is based on my observations and extended outboard of the main fault zones with the prior mapping of the region by *Dohrenwend* [1982a, 1982b] and *Ekren and Byers* [1985a, 1985b, 1986a, 1986b]. For those fault areas not previously the focus of Quaternary mapping, I used U.S. Geological Survey Orthophotoquads to extend mapping away from the regions covered by air photographs along the fault zones.

[17] Radiocarbon dating of organic materials and presence of tephra deposits are used when available to place limits on the age of geologic units. The results, methodology, and laboratory used for radiocarbon analysis are summarized in Table 1. The identification of tephras is provided by the Tephrochronology Laboratory at the United States Geological Survey in Menlo Park that is overseen by A. M. Sarna-Wojcicki. The method of analysis is described by *Sarna-Wojcicki and Davis* [1991] and results of samples collected in this study are summarized in Table 2.

[18] The degree of soil development is also used to assess the relative age of Quaternary alluvial surfaces to help in placing bounds on fault slip rate. Soil nomenclature follows that outlined by *Birkeland* [1999]. I limit attention primarily to the thickness, structure, and relative clay content and carbonate development of B horizons, all of which have been observed to increase as a function of time [e.g., *Birkeland*, 1999; *Harden*, 1982; *Machette*, 1978].

[19] An approximation of the most recent earthquake displacement may be extracted from the morphology of single-event fault scarps. The topographic expression of a fault scarp degrades in a systematic manner as a function of time and initial scarp height [*Bucknam and Anderson*, 1979; *Wallace*, 1977]. *Hanks and Wallace* [1985] represent the

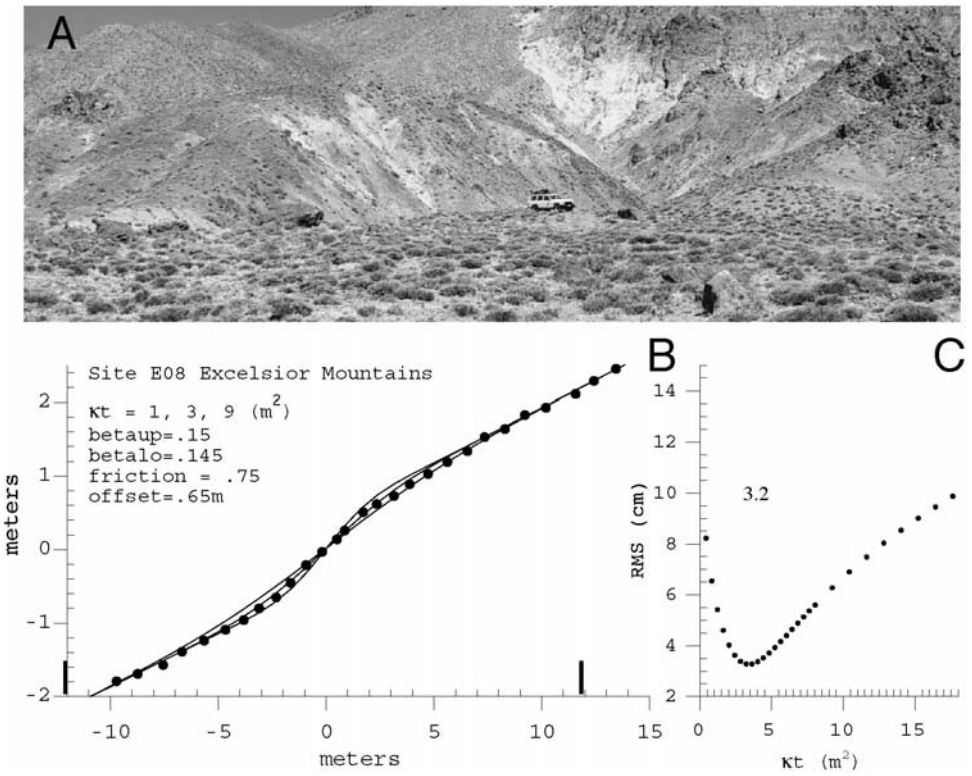

Figure 10. (a) Vehicle sits on scarp in young alluvium at Site E08 along southeast flank of Excelsior Mountains. Location is also annotated on Figure 9. (b) Measured (dots) and synthetic profile (lines) of scarp at Site E08 computed for values of κt listed, which are those that yield the best fit of the synthetic to the observed profile and two bounding values of κt. Listed are the assumed value of friction, the offset, and the values of betaup and betalo (the slopes of the footwall and hanging wall surfaces, respectively) used to compute the synthetic profiles. (c) Root-mean-square misfits of synthetic to observed profiles as a function of κt, computed for points ±12 m from middle of scarp. The value of $\kappa t = 3.2$ resulting in the minimum misfit is listed. The result supports a Holocene origin for the scarp when assuming $\kappa t = 1.1$.

process of scarp degradation using the diffusion equation which, expressed in the homogeneous form with constant coefficients, is written $du/dt - \kappa(d^2t/dx^2) = 0$, where u(x, t) is the elevation of a point on the scarp at time = t, x is the horizontal (cross-fault strike) distance, and κ is a constant of proportionality with the units of diffusivity in m^2/ky. The solution to the equation for the case where far-field slopes of the foot and hanging wall surfaces are not zero is delivered in detail by *Hanks and Andrews* [1989]. The solution provides the capability to formulate synthetic scarp profiles for specific values of product of the diffusivity and time (κt) that may be compared directly to measured scarp profiles. I also use this approach along fault scarps to produce synthetic scarp profiles that match those observed and, then, draw on an independent estimate that scarp diffusivity κ is about 1.1 [*Hanks and Wallace*, 1985] to place bounds on the age of the most recent surface rupture earthquake.

3.2. Rattlesnake Fault

[20] The Rattlesnake fault (Figure 2) strikes ~N75°E and is about 20 km in length (Figure 3). Quaternary displacement on the fault was first reported by *Bucknam*

Figure 11. Trace of the 1934 Excelsior Mountain earthquake remaining evident in bedrock 70 years after the event as alignment of small fissures and benches. Map board (~30 cm) aligned along strike provides scale.

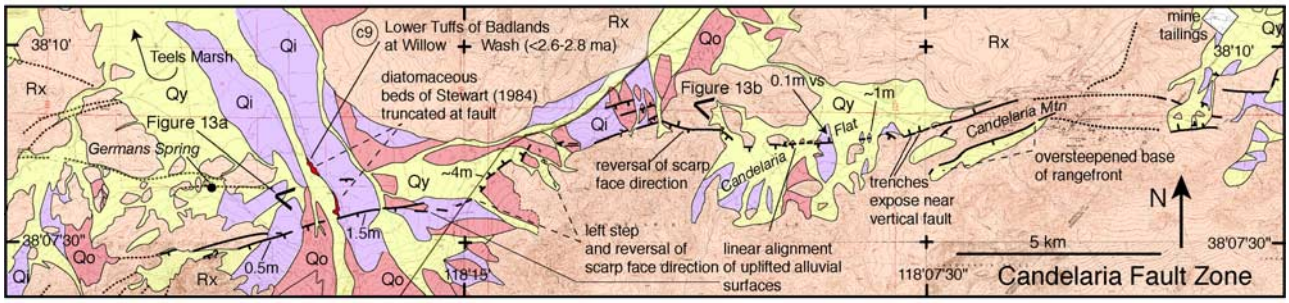

Figure 12. Candelaria fault trace and distribution of Quaternary deposits. Annotations show scarp heights and measures of vertical separation (vs). See Figure 3 and text for further explanation. Direction of view for photos in Figure 13 is indicated by open end of solid rotated V shapes.

[1974]. He suggested a left-lateral strike-slip origin for the fault based on the orientation, linearity, and geomorphic expression of the fault. Apparent left-lateral offsets of Tertiary basalts across the fault are evident in later regional geologic maps [*Carlson et al.*, 1978; *Garside*, 1982; *Stewart*, 1978; *Stewart et al.*, 1984]. The trace cuts from Rattlesnake Flat in the west through a drainage divide to Garfield Flat in the east (Figure 3). The fault trace is quite linear, often contained within bedrock, and forms linear enclosed depressions, uphill and alternately facing scarps, side hill benches and linear fault-bounded ridges (Figure 4), indicative of lateral slip. The westernmost strand of the fault bends to the south along a bedrock-alluvial contact and produces an oversteepening of the base of the range front, more suggestive of normal faulting (Figure 4b). About 2 miles (3 km) east of the drainage divide, between Rattlesnake and Garfield flats, a left stepping en echelon arrangement of several pressure ridges, the deflection of several drainages, and a beheaded stream channel are preserved in young alluvium and demonstrate youthful left-lateral offset (Figure 5). The active fault trace continues eastward into Garfield Flat where it produces uphill-facing scarps in young alluvium (unit Qy) and either ends or is obscured by active fan deposits to the south of the Garfield Flat playa, where it may also step further southward to continue along the north flank of the Excelsior mountains (Figure 3) [*Garside*, 1982]. The depression that marks Rattlesnake Flat reflects extension associated with the left bend and termination of the fault. The location of Garfield Flat is probably, at least in part, due to a similar accommodation of extension at the northeast terminus of the fault.

3.3. Anchorite Hills Fault Zone and North Mono Basin Escarpment

[21] The Anchorite Hills fault appears to be an extension of the normal fault that bounds the east flank of the Wassuk Range (Figure 2). Scarps along the Anchorite Hills fault zone average N60°E strike and extend southwestward from Anchorite Pass into the northern Mono Basin (Figure 6). Faulting within the Anchorite Hills is generally confined to volcanic bedrock and characterized by subparallel and abrupt escarpments that locally display opposite senses of throw along their length. *Gilbert et al.* [1968] document an ~300-m left-lateral separation of a 2.5 Ma andesite flow to estimate a slip rate of ~0.12 mm/yr (Figure 6). The fault displaces recessional shorelines of Pleistocene Lake Russell which has since desiccated to the current level of Mono Lake. Scarps within the Mono Basin trend more northerly than the overall strike of the zone, range up to about 1.5 m in height, and face both northeast and southwest. The low amplitude and broad crests of the bars on which the scarps are preserved and a loose veneer of young pumiceous ash that mantles the area hinder observation of any lateral component of offset. Asymmetry of scarp heights across lacustrine berm crests is suggestive of left-lateral offset. The sum of observations indicates a relatively long-lived left-lateral fault that continues to be active in the Holocene.

[22] The Mono Basin has been dominated by subsidence during the Quaternary. Subsidence has been accomplished primarily by normal faults along the Sierra Nevada front to the west and flexure along the remaining three sides [*Gilbert et al.*, 1968]. Up to ~1800 m of structural relief across the western portion of the Basin postdates the earliest recorded Sierra glaciations at about 3 Ma [*Gilbert et al.*, 1968]. Flexure along the North Mono Basin Escarpment (Figure 6) has produced at least ~300 m of structural relief subsequent to deposition of glacial gravels near Conway Summit. The displaced glacial gravels are interpreted by *Wahrhaftig and Sharp* [1965] to be of Sherwin age (>0.76 Ma [e.g., *Sarna-Wojcicki et al.*, 1991]). My examination of the North Mono Basin Escarpment reveals only a few lineaments and small scarps that break lacustrine deposits of Lake Russell (Figure 6). The few scarps commonly face uphill, locally strike at high angle to the edge of the basin, and display a weak en echelon arrangement. The arrangement of scarps may accommodate a component of left-lateral shear and hence a continuation of the type of displacement observed along the Anchorite Hills fault zone. That the fault zone is not well expressed may also reflect that deformation is accommodated by warping [*Gilbert et al.*, 1968] or volcanic processes [*Bursik and Sieh*, 1989]. As well, some scarps may have avoided recognition where they strike parallel to beach ridges.

3.4. Huntoon Valley

[23] The Huntoon Valley is a fault bounded basin within the Excelsior Mountains. The valley trends northeast a

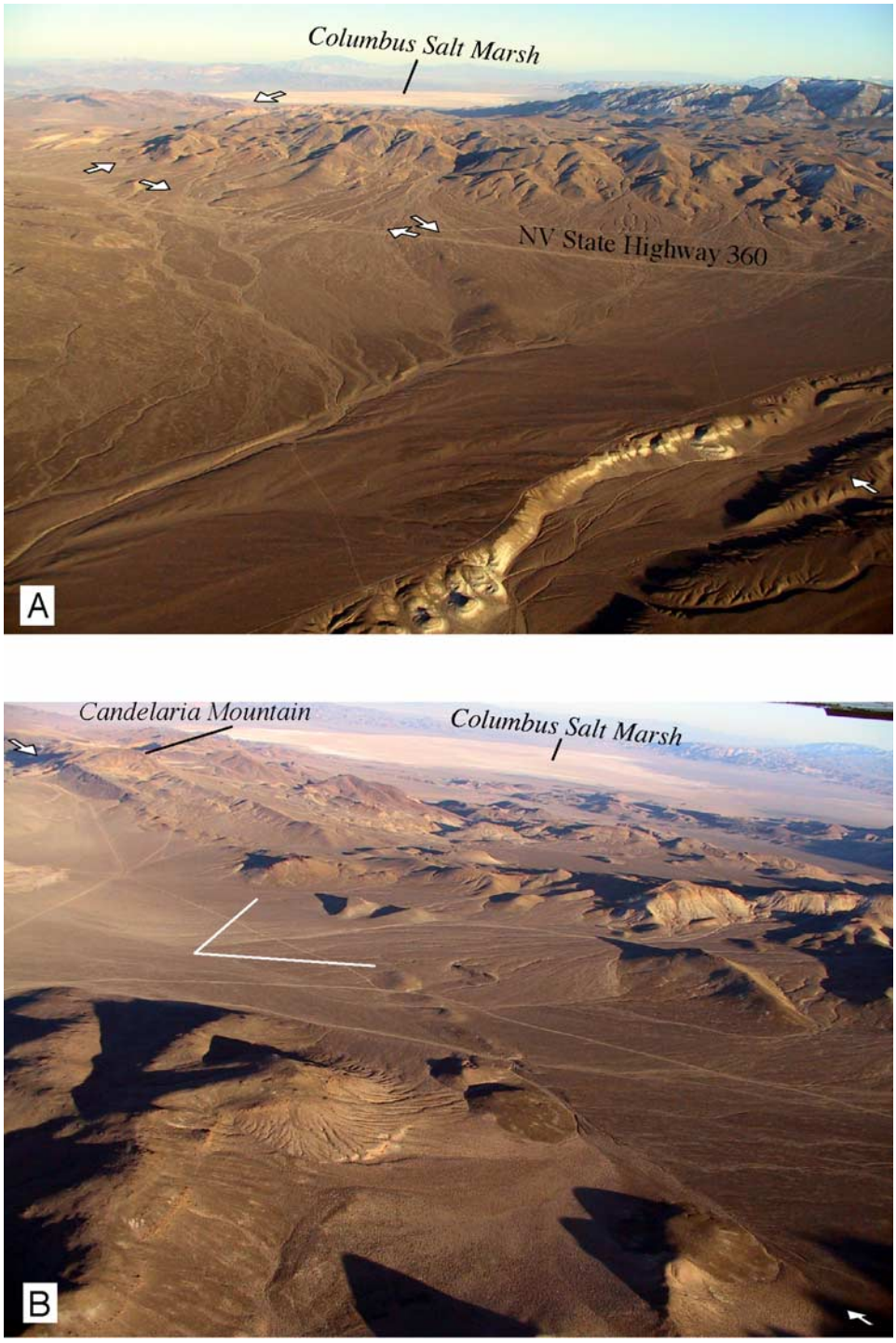

Figure 13. Candelaria fault. (a) Eastward view. Sections of fault are delineated by opposite facing arrows. Western section (nearest) is marked by linear arrangement of alluvial ridges and uphill south facing scarps. Central section delineates a left bend in the fault trace and a normal sense of displacement with scarps consistently facing northwest. (b) Easternmost section. View is to southwest. Strike of western section of fault is defined by aligned linear ridges and alluvial and bedrock knobs (between white arrows). Section of fault in Candelaria Flat that shows Holocene offset is delineated by open end of white V. Perspective of photos is annotated in Figure 12.

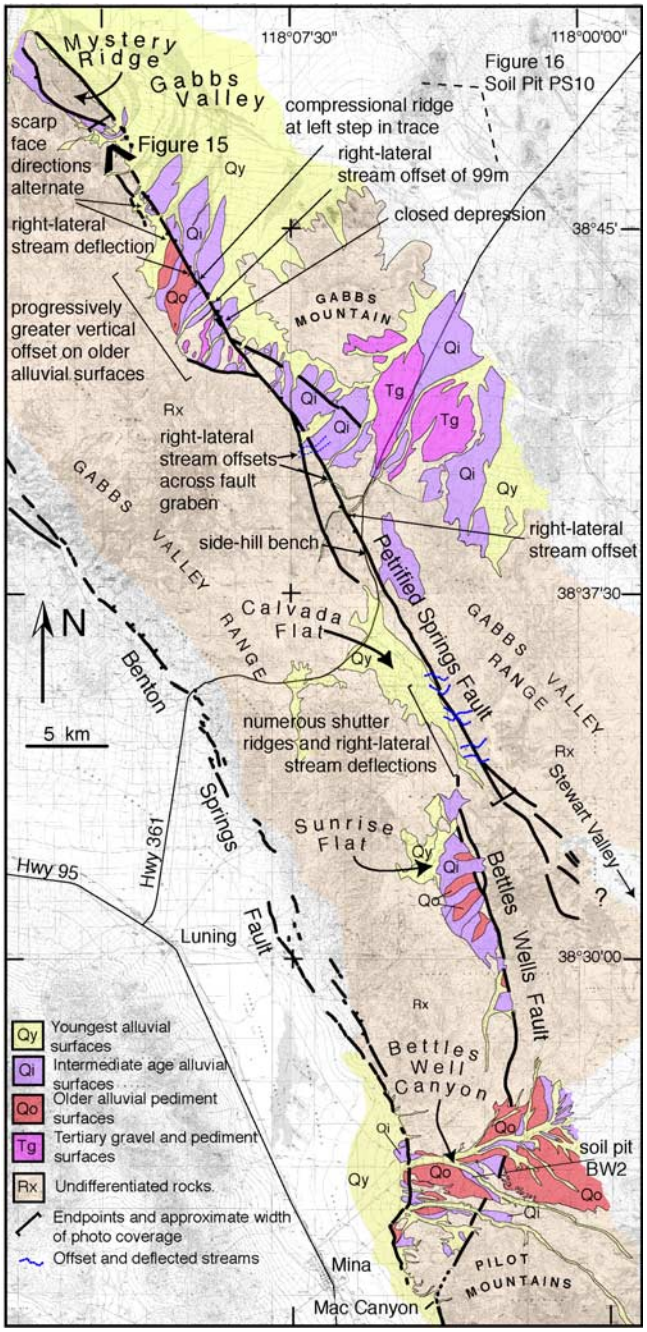

Figure 14. Petrified Springs fault trace. The fault trace (bold lines) is annotated to mark features indicative of lateral offset and ongoing fault activity. Location of map in Figure 16 and soil pit PS10 are also labeled. Perspective of photo in Figure 15 is shown by bold open ended V shape. Units Qy, Qi, and Qo are Quaternary surfaces of relatively increasing age. Units Tg and Rx encompass Tertiary gravels and undifferentiated bedrock, respectively. See text for further discussion. Details of Benton Springs fault are shown in Figure 19.

distance of ~16 km and is bounded by the Adobe Hills to the southeast (Figures 2 and 7). The abruptness of the escarpments bounding both sides of the valley gave *Stewart et al.* [1981] reason to infer the basin is fault bounded. There is little sign of recent fault activity other than local occurrences of oversteepening at the base of the range front and a number of well-developed triangular facets on the northwest side of the valley. The alluvial apron along the northwest side of the valley also appears to lack young fault scarps (Figure 7). Fan head trenches at two sites along the northwest margin expose Mono ash layers that probably date to about 900 to 1000 ^{14}C years B.P. (samples SGW-HW21 and SGW-HW13, Table 2 and Figure 7). The ash layers sit beneath a thin veneer of fan alluvium and desert pavement, approach 0.5 m in thickness, and are exposed continuously over ~20–30 m distance. The presence and geometry of the ash beds confirms the active nature and young age of the fan deposits that form the alluvial apron blanketing the northwest flank of the basin. The only remnant of fault displacement in alluvium is a small triangular patch of alluvium at the northern end of the valley. The remnant displays an argillic soil horizon and stage 3+ carbonate development and is lifted ~4 m out of grade by an uphill facing scarp. The northeastern flank of the valley is draped by aeolian deposits which may obscure any young displacements.

[24] Scarps in alluvium are present along the southeastern margin of the valley. The scarps cut and bound a pediment surface at their most northeastern extent (Figure 7). The pediment is constructed on white to light gray fine-grained diatomaceous and tuff-bearing sediment. The tuff (sample SGW-HE17, Figure 7) is correlated to previously identified tuffs of about <2.56 to 2.8 Ma (Table 2). Fringing accumulations of lacustrine sediment form a distinct set of shorelines along a basalt cliff near and at the same elevation as the alluvial scarps. The alluvial scarps are probably wave-cut features. To summarize, the few scarps preserved in alluvium appear limited to pre-Holocene surfaces and may not be of tectonic origin. Active fan deposition and aeolian reworking of those deposits may obscure fault scarps in younger deposits. The bounding escarpments suggest the dominant sense of range-bounding faulting is normal. *Gilbert et al.*'s [1968] observations of subhorizontal slickensides on bedrock faults at the southeast end of Huntoon Valley permits an oblique component as well. Little Huntoon Valley to the north shares the same characteristics.

3.5. Excelsior Mountains

[25] The south and east flanks of the Excelsior Mountains are fault bounded (Figure 8). The region is included in numerous geologic maps [*Dohrenwend*, 1982a; *Garside*, 1982; *Stewart*, 1984; *Stewart et al.*, 1982]. The fault strikes northerly ~13 km from its southwestern end to about latitude 38°15′N. Faulting along this section is distributed between a number of subparallel and curvilinear fault traces. Scarps face eastward and truncate uplifted intermediate and older fan and pediment surfaces. The fault then bends 90° to strike east where it displays a relatively linear and singular trace (Figure 9a). Fault scarps face south within Teels

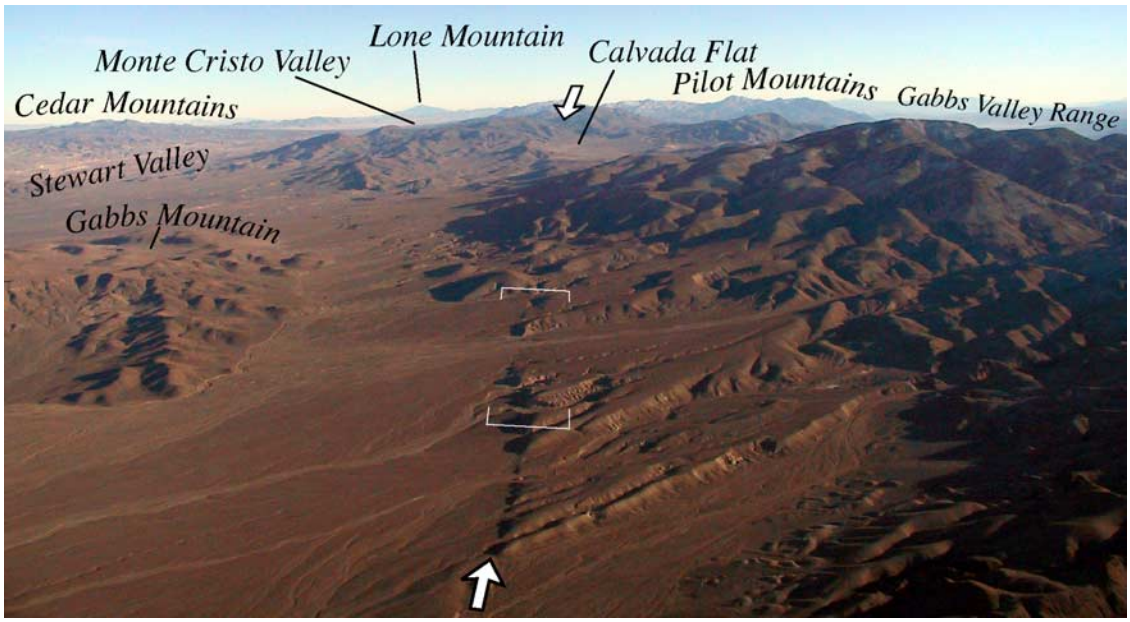

Figure 15. View southeast along strike of Petrified Springs fault trace (between white arrows). Vantage point of photo is shown in Figure 14. Brackets show approximate extent of photo and strip map in Figure 16.

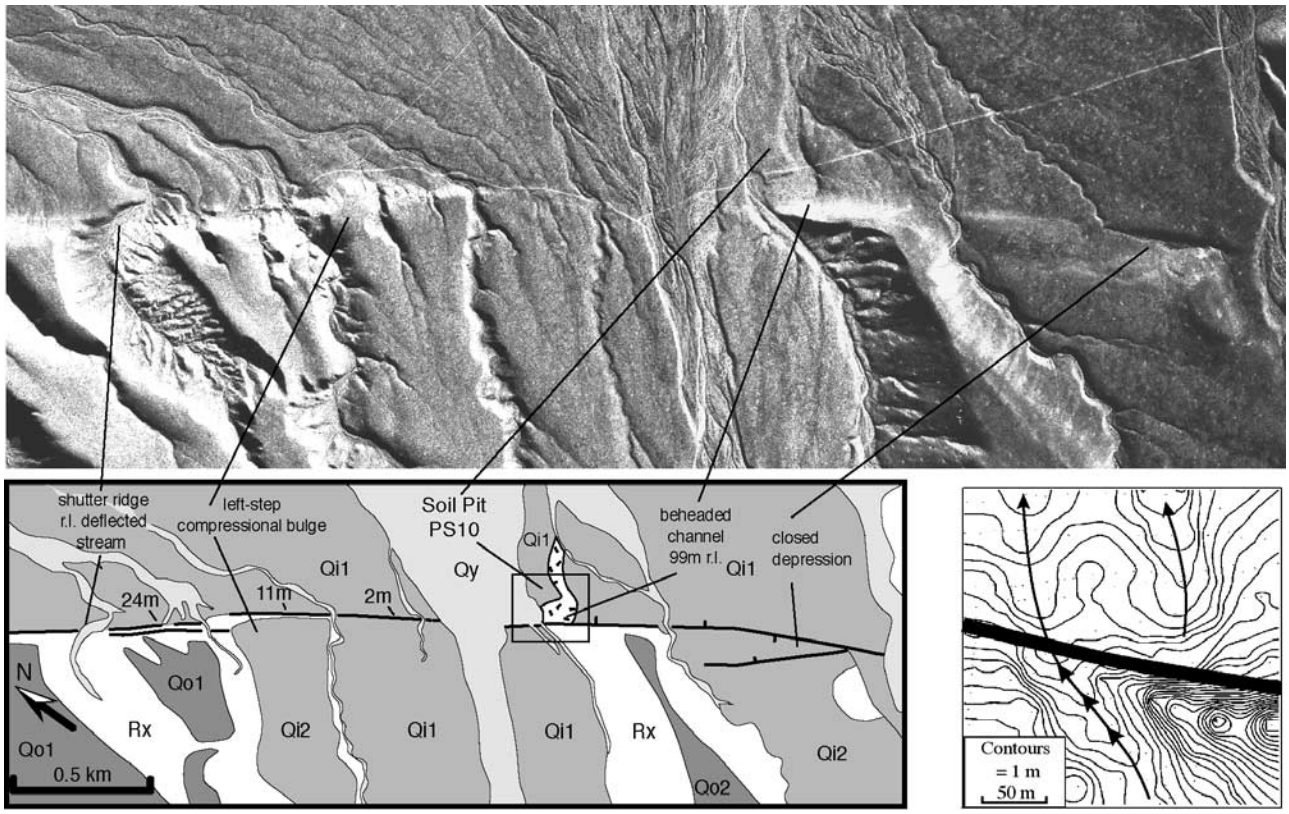

Figure 16. Photo and sketch map of Quaternary surfaces, scarp heights, and features indicative of active faulting along a section of the Petrified Springs fault trace adjacent to Gabbs Valley. Contour map at 1-m interval (lower right) documents probable ~99 m right-lateral offset of stream channel. Location also is shown in Figure 14. Units Qy, Qi, and Qo are Quaternary surfaces of relatively increasing age (see text for discussion). Subunits of relatively increasing age are further annotated with 1 and 2, respectively.

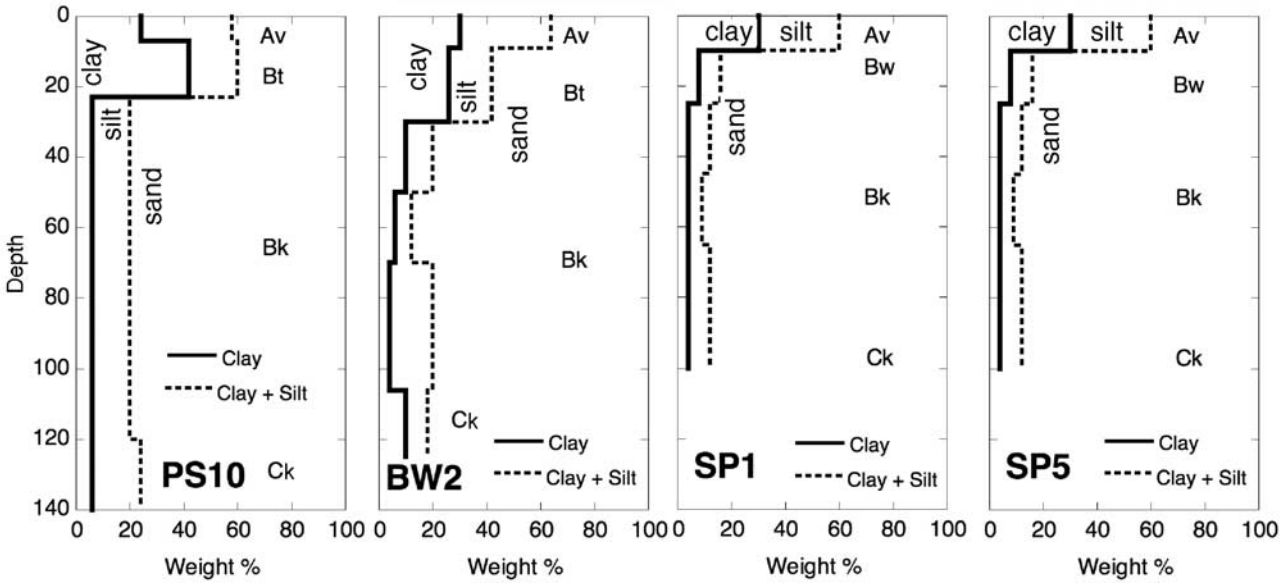

Figure 17. Soil texture profiles showing weight percent of clay, silt, and sand as a function of depth. Locations of profiles BW2 along Bettles Well fault and PS10 are shown in Figures 14 and 16 and profiles SP1 and SP5 are shown in Figures 19 and 22. Coordinates (UTM NAD 27 CONUS) of localities are PS10, 0399304 4286600; BW2, 0406469 4252450; SP1, 0406356 4252531; SP5, 0406269 4252401.

Figure 18. View south along Benton Springs fault from Rhyolite Pass. The fault trace (between arrows) strikes southward along a longitudinal valley, gradually bends right to flank the west flank of the Gabbs Valley Range, and then takes an abrupt right bend at Bettles Wells Canyon before continuing along the west flank of the Pilot Mountains. Perspective of photo is shown on map in Figure 19.

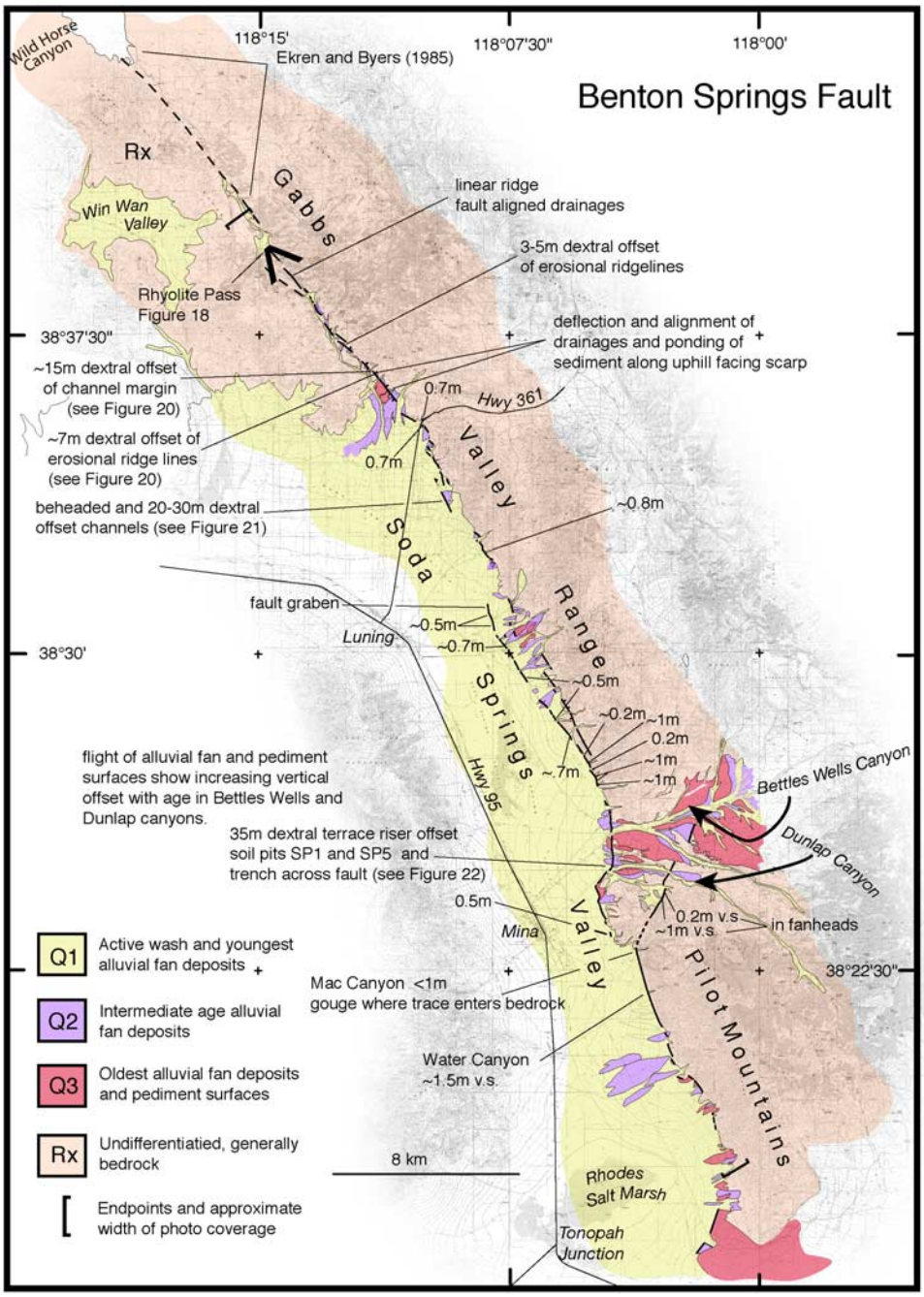

Figure 19. Map of Benton Springs fault trace. Numerical annotations are scarp height unless specifically indicated to be vertical separation (vs) or dextral. Perspective of photo in Figure 18 is shown by open ended V shape. Locations of maps in Figures 20, 21, and 22 are marked. Units Qy, Qi, and Qo are Quaternary surfaces of relatively increasing age. The older alluvial surfaces (Qo) at the southern end of the Pilot Mountains overlie Pliocene lake beds [*Reheis et al.*, 2002]. See text for further discussion.

Marsh. Where the fault enters the pass separating Teels Marsh from Rhodes Salt Marsh, a reversal in scarp direction occurs and the fault locally produces a side hill bench (Figures 8 and 9b). At about 118°15′W longitude, the fault trace bifurcates. The trace that continues linearly to the east is discontinuous, interacts with alluvial fan remnants on the edges of Rhodes Salt Marsh, and shows north facing scarps. The remaining trace bends sharply and curves northwest along the main Excelsior range front. Alluvial scarps along this trace face southeastward away from the mountain. In sum, the curvilinear traces bounding the Excelsior Mountains on the western edges of Teels Marsh and Rhodes Salt

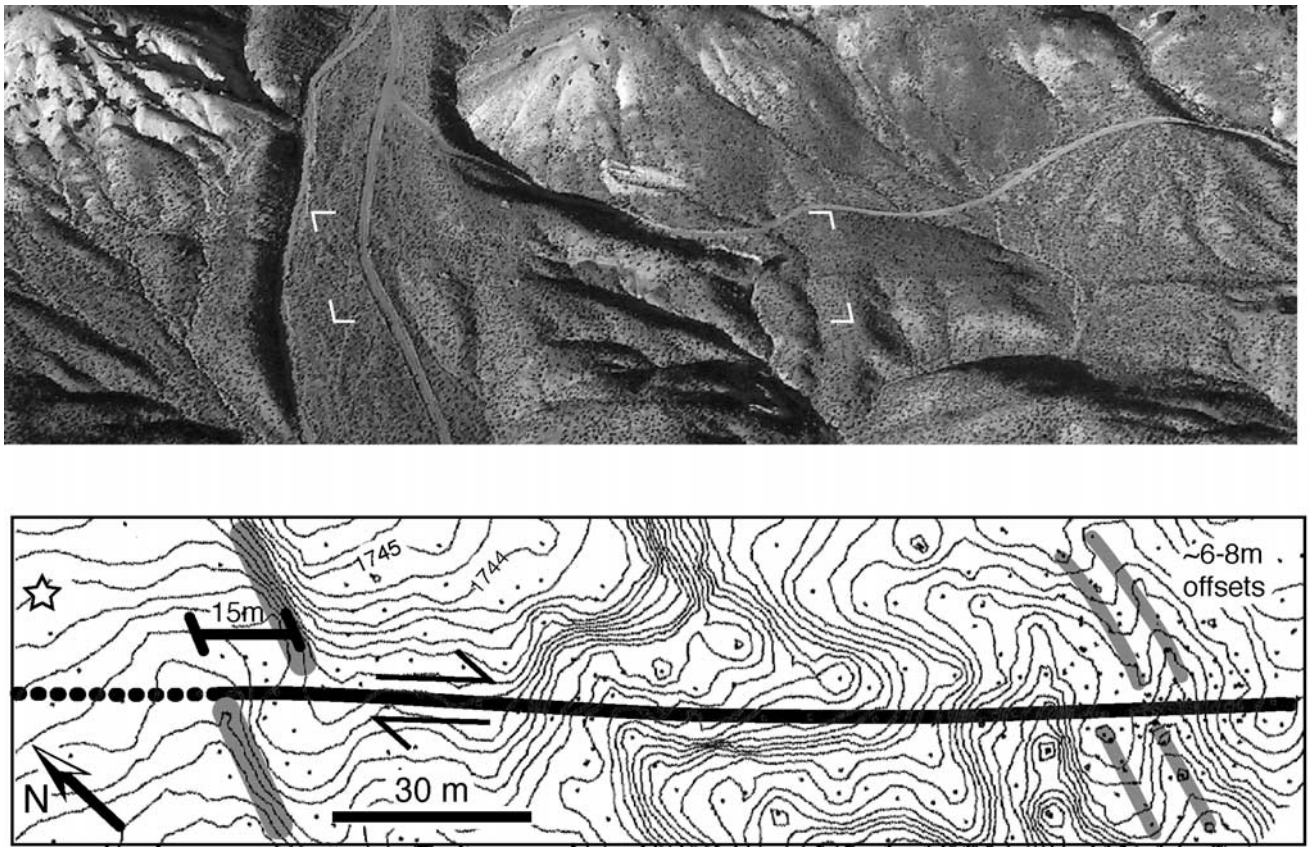

Figure 20. Photo and 0.5 m contour interval map of (shaded) right-lateral offsets of channels, channel margins, and ridgelines along the northern section of the Benton Springs fault. Extent of contour map is shown by white brackets in photo. Coordinates (UTM NAD27 CONUS) of point marked by star are E396102 N4274096. Figure location is also shown in Figure 19.

Marsh exhibit the characteristics of a range bounding normal fault. The linearity of the central portion of the fault zone and the reversal of scarp sense as it cuts through the high mountain saddle at 118°15′ latitude is consistent with a large component of strike slip. The Teels and Rhodes Salt Marsh basins appear to be the result of extension at the ends of a left-lateral strike-slip fault.

[26] The trace follows a bedrock-alluvial contact and extends southward to cut alluvium at site E33 near the southern end of the trace (Figure 8). The offset surface exhibits weak soil development, lacks an argillic horizon and shows stage 1 carbonate development. The observations suggest that the age of the most recent offset and some elements of the Qi surface that is displaced south of site E33 are Holocene in age. *Garside* [1982] reported a 3590 ± 100 ^{14}C years B.P. age (conventional) for peat deposits offset by a splay of the fault system at about 118°15′ longitude along the northwestern end of Teels Marsh (Figure 8). I sampled a faulted peat deposit along the same trace. The sample yielded an accelerator mass spectrometry (AMS) age of 1415 ± 45 ^{14}C years B.P. (Table 1 and Figure 8, sample T5-C). Farther east, a small single-event scarp of about 0.6 m height cuts a fan head along the northeast striking trace bounding Rhodes Salt Marsh (site E08 in Figure 8). The faulted fan is a boulder gravel, maintains a muted bar and swale topography, and the surface characteristics match across the fault scarp. The surface morphology and shape of a scarp profile at site E08 indicates the scarp was formed during middle to late Holocene time (Figure 10). The sum of observations indicate the fault is active in the Holocene and suggest displacement is largely strike slip along the east trending portion of the trace.

[27] Longer-term displacement is evident in truncated and uplifted older fan and pediment surfaces within Teels Marsh (Figure 8). At one locality (sample SGW-TA1a in Figure 8), pediment gravels mapped by *Stewart* [1984] at the northwestern corner of Teels Marsh form a strath that is now 50–60 m above modern stream grade and rests unconformably on sedimentary beds that dip ~20°W. A tephra exposed in the tilted sedimentary beds along the adjacent wash (sample TA1a) is most chemically similar to a 3.4 Ma tephra previously identified nearby (Table 2 and Figure 8). The observations place a minimum bound on the uplift rate of about 0.01 mm/yr, assuming the relative uplift is due solely to tectonic input.

[28] The Excelsior Mountains were the site of a moderate M = 6.5 earthquake in 1934 [*Doser*, 1988]. The earthquake

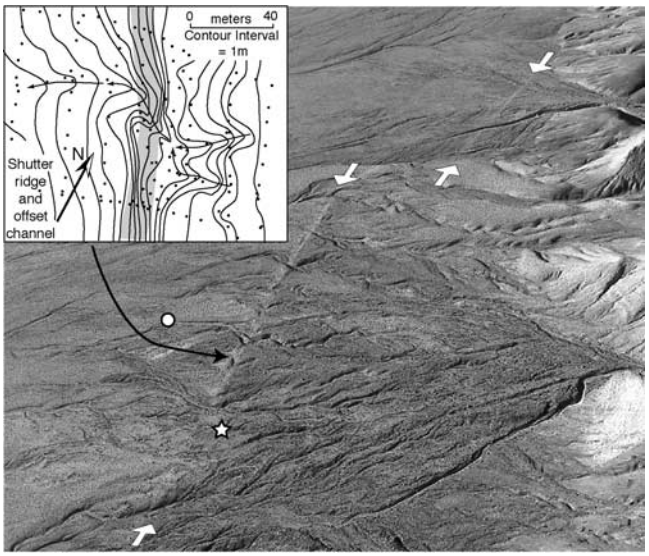

Figure 21. Photo and contour map showing linearity of trace (between arrows), shutter ridges, and offset channels along section of Benton Springs fault in northern Soda Springs Valley. View is to northwest. Contour map documents shutter ridge and ~30 m right-lateral offset of drainage channel in alluvium. Trend of scarp is shaded. White dot on photo sits at end of prominent beheaded and right laterally offset channel. Coordinates (UTM NAD 27 CONUS) of point marked by star are ~N4268150 E399325. Location is also annotated in Figure 19.

produced a ~1-km-long break of the ground surface within the Excelsior Mountains (Figure 8) [*Callaghan and Gianella*, 1935]. *Callaghan and Gianella* [1935] report the earthquake break occurred along a preexisting N65°E fault zone and exhibited scarps of maximum ~13 cm height and fissure openings up to ~8 cm. They further report the normal component of movement was consistently down to the north and describe an en echelon pattern of fractures consistent with a left-lateral component of displacement. Analysis of limited seismological observations suggest the event produced primarily normal displacement [*Doser*, 1988]. A recent visit shows the scarps and fissures remain well preserved in bedrock (Figure 11). The earthquake that produced the scarp does not appear to be due to slip on the main range-bounding fault.

3.6. Candelaria Fault Zone

[29] The trace of the Candelaria fault zone appears on the maps of *Dohrenwend* [1982a], *Stewart* [1981, 1984], and *Stewart et al.* [1982]. *Speed and Cogbill* [1979] pointed out the active nature of the fault, and combined observations of fault striae and measurable throw of Pliocene basalts to estimate a cumulative 900 m of net left-oblique slip since 2.8 Ma, about 0.3 mm/yr. (Figure 12). The westernmost section of the fault displays aligned ridges and uphill south facing scarps (Figure 13a). The fault truncates a sequence of white flat-lying volcanic ash-bearing diatomaceous beds buried beneath alluvium of intermediate age along the eastern cut bank of the large drainage entering Teels Marsh (Figures 12 and 13a) [*Stewart*, 1984]. The ash (sample SGW-C9 T492) most likely correlates to the 2.6–2.8 Ma Lower Tuffs of Badlands at Willow Wash (Table 2). The easterly strike of the fault is interrupted by a northward bend at about 118°15′. The fault traces a normal scarp that faces northwest within the bend. Eastward, the fault again displays strike-slip morphology consisting of uplifted alluvial knobs and the alternation of scarp-facing directions along strike (Figure 13b). The normal expression of the fault within the left bend is that expected for young left-lateral displacements extending away from the bend [e.g., *Crowell*, 1974]. The eastern and western endpoints of the active fault trace appear to diminish in bedrock and are not well defined. Small ~0.1-m scarps break elements of the active fan apron in Candelaria Flat (Figures 12 and 13b). The broken fan surfaces are capped by a continuous loose pavement of pebble clasts. Disruption of the pavement remains evident and changes in vegetation are common along the disruption. The displacement and preservation of the delicate geomorphic features on young fan surfaces suggest a middle to late Holocene age for the most recent displacement.

3.7. Petrified Springs Fault

[30] Prior Quaternary and bedrock geology maps of the Petrified Springs fault include *Ekren and Byers* [1985a] and *Dohrenwend* [1982a]. The tuffs of Mount Ferguson show apparent right-lateral offset of ~12 km across the fault (Figure 2), and *Ekren and Byers* [1984] suggest 16 km of right-lateral offset is probable based on a more regional analysis of the distribution of Miocene tuffs. The fault is the easternmost of the northeast trending strike-slip faults in the Walker Lane. From a northern limit at Mystery Ridge, the fault strikes southward about 30 km to Calvada Flat (Figure 14). Linear valleys and ridges, deflected and laterally offset streams, side hill benches, scarp face reversals, closed depressions, compressional ridges, and vegetation lineaments occur along the linear trace (Figures 14 and 15). A larger-scale photo and sketch map of a portion of the fault along the west edge of Gabbs Valley illustrates some of these features (Figure 16). On the sketch map, the trace adjacent to Gabbs Valley is linear, the scarp generally faces northeast, and a vertical component of motion has uplifted a set of alluvial fan and pediment surfaces. The surfaces show increasing amounts of uplift as a function of relative age. A linear closed depression occurs along the southeastern end of the map area. A small left step in trace is associated with a compressional ridge or "push-up" in the northern section of the same map area. A beheaded stream incised into a Qi surface appears to record ~99 m of right-lateral offset (Figure 16).

[31] The alluvial surface that records the 99 m offset is composed of broad interfluves covered by a relatively continuous pavement of darkly varnished subangular to subrounded volcanic clasts. A soil chronosequence for a similar set of abandoned alluvial terraces has been previously developed about 20 miles (32 km) to the south in

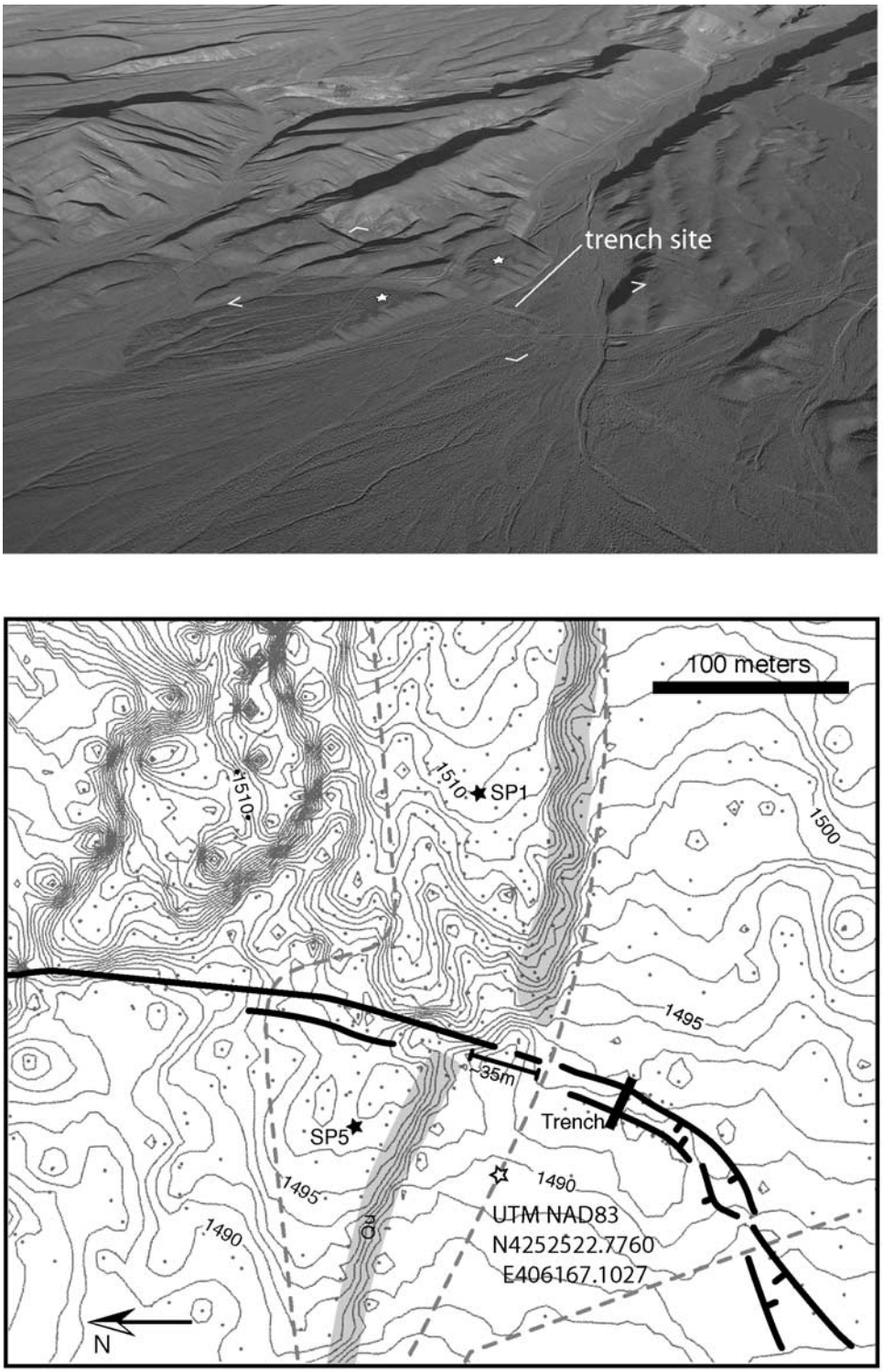

Figure 22. Photo and map of dextrally offset terrace riser along the Benton Springs fault (bold lines) at Dunlap Canyon. Approximate extent of contour map is marked by white corner brackets in photo. Shaded zones in contour map highlight channel margin. Locations of soil texture profiles SP1 and SP5 shown in Figure 17 are denoted by white stars on photo and black stars on map. Sketch of trench site is presented in Figure 23. Site location given by UTM coordinates (open star on map) and location also marked in Figure 19.

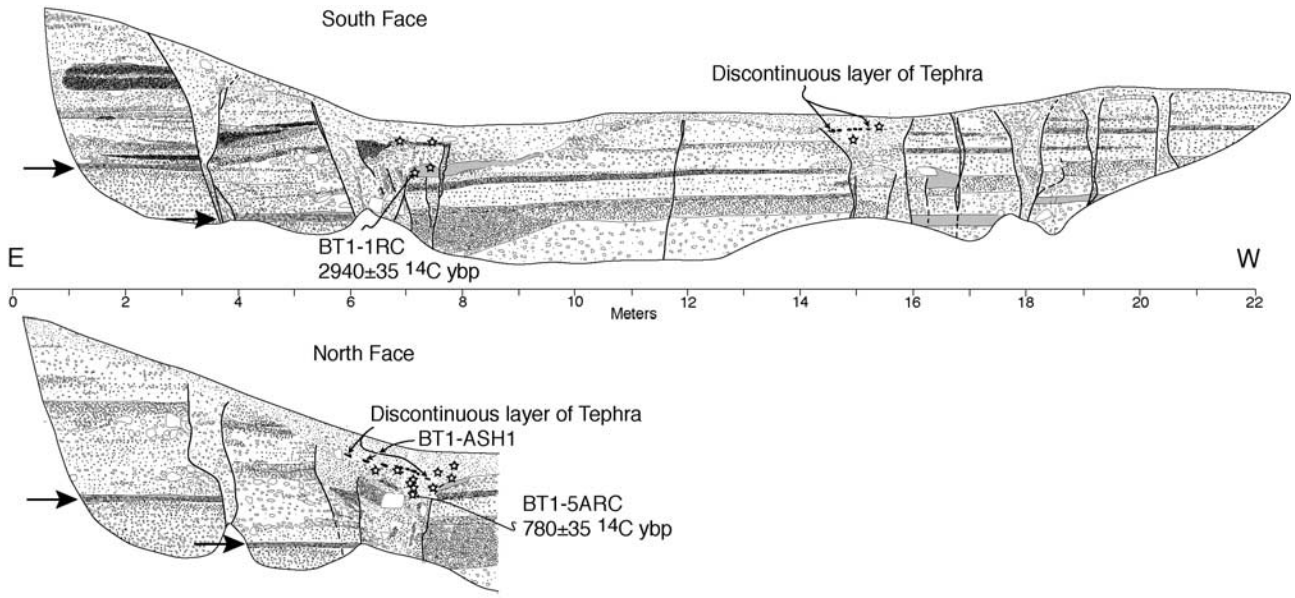

Figure 23. Sketch of trench exposure shows alluvial packages displaced by graben-forming fault strands (bold lines) of Benton Springs fault at Dunlap Canyon. The presence of Mono tephra and dating of charcoal (stars) in colluvium shed off the scarp produced by the last displacement indicate a surface rupture earthquake during the last ~1000 years. Horizontal arrows show down-to-west displacement of distinct layer. See text for discussion.

Bettles Wells Canyon [*Bell*, 1995; *Bell et al.*, 1999]. Pits excavated into the Qi1 surface (PS10 in Figure 16) and a surface correlated to be <60–90 ka in Bettles Wells Canyon (Qf2a surface of *Bell* [1995]) show similar pedogenic profiles (Figure 17). Each displays reddened 15–20 cm thick Bt horizons of moderate structural grade and underlying Bk horizons with stage II+ carbonate development. Assuming the two surfaces are similar in age and the entirety of the 99 m offset is tectonic in origin, the observations point to a minimum right-lateral slip rate of 1.1 to 1.65 mm/yr, a reasonable value given the robust geomorphic expression of the fault.

[32] Shutter ridges and right-lateral stream deflections are numerous along the section of fault between Gabbs Valley and Calvada Flat where the trace is mostly confined to bedrock. (Figure 14). The fault trace bifurcates at the southern end of Calvada Flat. *Ekren and Byers* [1984] project the northern strand a distance of ~10 km and into Stewart Valley, somewhat on strike with a discontinuous zone of right-lateral surface fractures produced by the 1932 Cedar Mountain earthquake (Figure 1). The southwestern strand is the Bettles Wells fault. It strikes more southerly and continues another 15–20 km along the east flank of Sunrise Flat toward the Pilot Mountains at which point it appears to merge with the Benton Springs fault. The linearity of the trace, side hill benches, and the alignment of bedrock knobs just outboard of the main range front are compatible with youthful displacement and a significant component of lateral slip along Sunrise Flat. Right-lateral displacements of older bedrock units are mapped along the section of fault between the alluvial deposits of Sunrise Flat and Bettles Wells Canyon [*Oldow and Meinwald*, 1992].

3.8. Benton Springs Fault

[33] The Benton Springs fault (Figure 2) is well expressed in Quaternary alluvium at sites along the ~50 km from Rhyolite Pass in the north to Rhodes Salt Marsh in the south (Figures 18 and 19). *Ekren and Byers* [1986b] infer the fault continues northward another 45 km beyond the Gabbs Valley Range to where it bounds the eastern flank of the Terrell Mountains. Right-lateral offset was recognized by *Ferguson and Muller* [1949]. Sections of the fault have since been mapped by *Ekren and Byers* [1985a, 1985b, 1986a, 1986b], *Dohrenwend* [1982a, 1982b], *Speed* [1981], and *Stewart et al.* [1982]. *Ekren and Byers* [1984] document a 6.4–9.6 km right offset of a steep contact of a Cretaceous granitic pluton (Figure 2) and an 8 km right offset of younger Tertiary tuffs. Lateral slip on the fault is entirely Tertiary and younger [*Ekren and Byers*, 1984; *Ferguson and Muller*, 1949].

[34] The fault is confined to the Gabbs Valley Range between Rhyolite Pass and Soda Springs Valley (Figure 19). Displacement has led to development of a narrow fault-aligned valley. Within the valley, linear ridges, fault-aligned drainages, offsets of erosional ridgelines and active channel margins show recent right-lateral strike slip (Figure 20). The fault runs along the west flank of the Gabbs Valley Range at the north end of Soda Springs Valley where it truncates an intermediate age fan or pediment surface of granitic composition, about 3.5 km south of State Highway 361. Beheaded

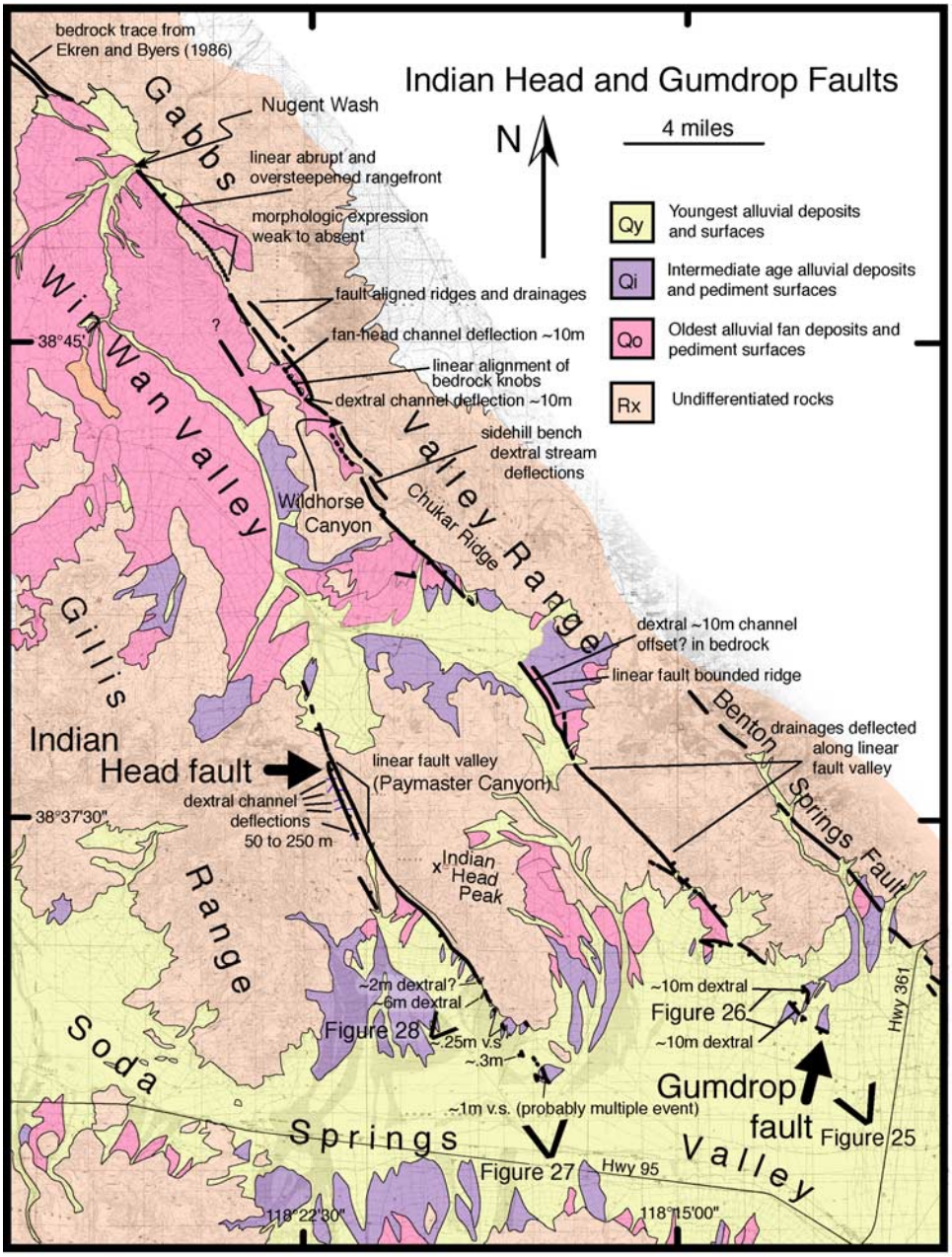

Figure 24. Traces of Indian Head and Gumdrop faults. Features indicative of lateral offset and ongoing fault activity are annotated. Perspectives of photo in Figures 25, 27, and 28 are shown by open ended V shapes. Units Qy, Qi, and Qo are Quaternary surfaces of relatively increasing age. Unit Rx is undifferentiated bedrock. See text for further discussion. See Figure 19 for detail of Benton Springs Fault.

channels and shutter ridges record up to 30 m of right-lateral displacement (Figure 21). Displacement occurs on two subparallel strands south of Luning (Figure 19). The western of the two strands has produced small grabens and generally west facing scarps in young alluvium. The fault trace bends sharply to the right between Bettles Wells and Dunlap Canyons. The vertical component of slip within the bend has resulted in the abandonment of alluvial fan and pediment surfaces that record increasing displacement as a function of age (Figure 19). A terrace riser cut into the surfaces at Dunlap Canyon also records ~35 m of right-lateral displacement (Figure 22). The offset surface is mapped as unit Q2fb by *Bell* [1995] and, on the basis of his development of a chronosequence, estimated to be <36 ka. Dividing the ~35 m offset by the <36 ka age of the offset surface places a minimum bound on the right-lateral fault slip rate of ~1 mm/yr. However, the unit Qf2b surface is defined in part by the development of 15- to 25-cm-thick loamy clay Bt horizons that are reddened and weakly prismatic (for example, profile BW2 in Figure 17) [*Bell*, 1995; *Bell et*

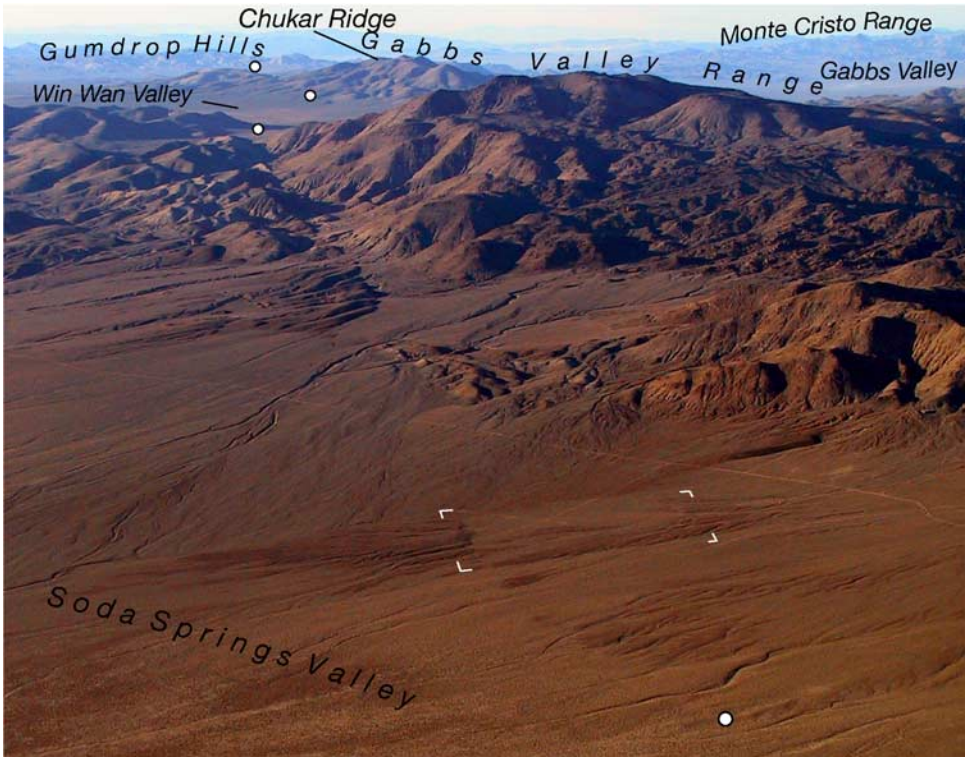

Figure 25. View north along trace (between white dots) of Gumdrop fault. Linear fault-controlled valleys mark the trace of the fault as it extends northward from Soda Springs Valley to Win Wan Flat, where the fault either bends or steps to the right and continues along the east flank of Chukar Ridge. Perspective of photo is shown in Figure 24. Corner angles outline photo in Figure 26.

al., 1999]. Soil texture profiles on the surface recording the offset are distinguished by a weaker soil lacking development of an argillic (Bt) horizon (profiles SP1 and SP5 in Figure 17 and 22). On that basis, the offset surface appears considerably younger than 36 ka, and hence the lateral slip rate is likely significantly higher than 1 mm/yr.

[35] A trench excavated across a fault graben at Dunlap Canyon exposed alluvial gravels displaced by the fault (Figure 22). The exposure consisted largely of subangular poorly sorted coarse sand and pebble alluvial fan gravel. The layer fabric is sketched to scale and fault displacements are shown in Figure 23. Distinct gravel beds may be

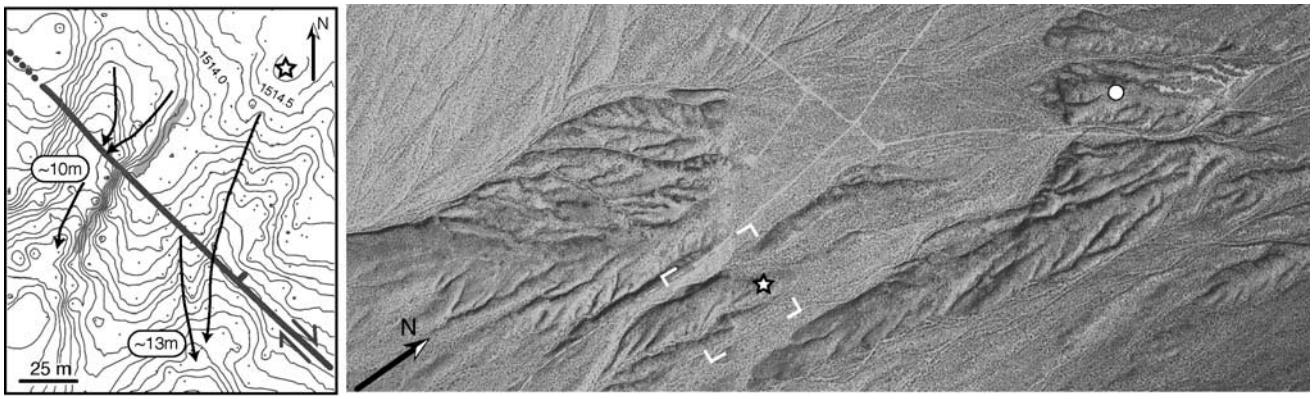

Figure 26. Aerial photo and 0.25 m contour map of dextral channel and channel margin offsets along subparallel strands of the Gumdrop fault in Soda Springs Valley. Brackets in air photo outline area of topographic map. Arrows delineate channels and flow directions. A channel margin (shaded) and beheaded channel are offset ~10 and ~13 m, respectively. Another dextral channel offset of about ~10 m is adjacent to white dot. UTM coordinate (UTM NAD 27 CONUS) of point marked by stars is N4270043 E394623. Location also noted on map in Figure 24.

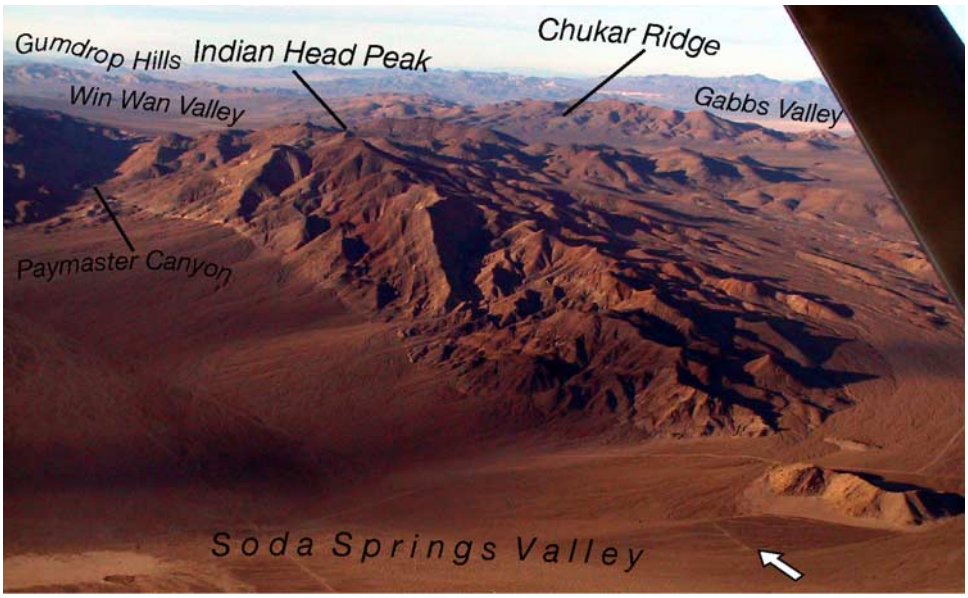

Figure 27. View north across Indian Head fault. Fault displaces late Pleistocene or Holocene deposits in Soda Springs Valley (arrow), forms a linear and abrupt range front as it strikes northwestward toward Indian Head Peak and into Paymaster Canyon. Perspective of photo is shown in Figure 24.

followed continuously across small down-to-the-east displacements from the west end of the trench to a fault contact and zone of shear at about meter 6 to 7. The fabric and facies of gravel east of meter 6 do not match that observed to the west. The mismatch reflects significant strike-slip motion. Displacement along shear zones at meters 4 and 6 has produced a west facing scarp. A gravel layer records apparent down-to-the-west normal displacement of $\sim$1 m across the fault at meter 4 (horizontal arrows in Figure 23). Upsection, facies mismatches across the same strand suggest the presence of a strike-slip component as well. The age of a small piece of charcoal (sample BT1-1RC) retrieved from a faulted massive fine sand layer on the south face shows the last displacement postdates 2940 $\pm$ 35 ^{14}C years B.P. (Table 1). A wedge of colluvium has developed above the shear zone at meter 6 to 7 since the last displacement. The colluvial wedge is thicker on the north face. There, small lenses of tephra form a discontinuous layer within the colluvium. Discrete pieces of charcoal reaching several millimeters in dimension and larger pods of burnt soil are also disseminated within and at the base of the colluvial wedge. The depth of preservation of both the tephra and charcoal within the wedge, the presence of burnt soil, and the lack of similar material in exposed footwall deposits suggest the charcoal was created, the tephra deposited, and both collected from

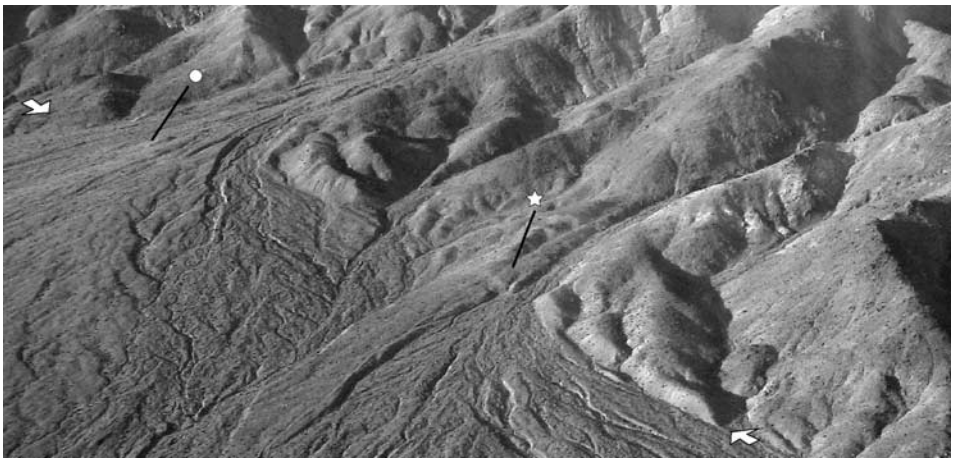

Figure 28. Oblique air photo of Indian Head fault trace (between arrows) along west flank of Indian Head Peak. Perspective of photo is annotated in Figure 24. Older elements of active fan preserve fault scarps (circle and star). Channel margin is dextrally offset $\sim$6 m along fault trace (star).

the surface and preserved in the colluvial wedge at or near the time of the earthquake, rather than being reworked from preexisting footwall deposits. The age of a piece of charcoal (sample BT1-5ARC) taken from the base of the colluvial wedge is 780 ± 35 ^{14}C years B.P. The ash (sample SGW-BT1-ASH1, Table 2) chemically correlates to numerous late Holocene ashes emitted from Mono Craters with a best, though statistically insignificant, fit for ash emitted ~800–1200 ^{14}C years B.P. The earthquake displacement and eruption may well have been coeval.

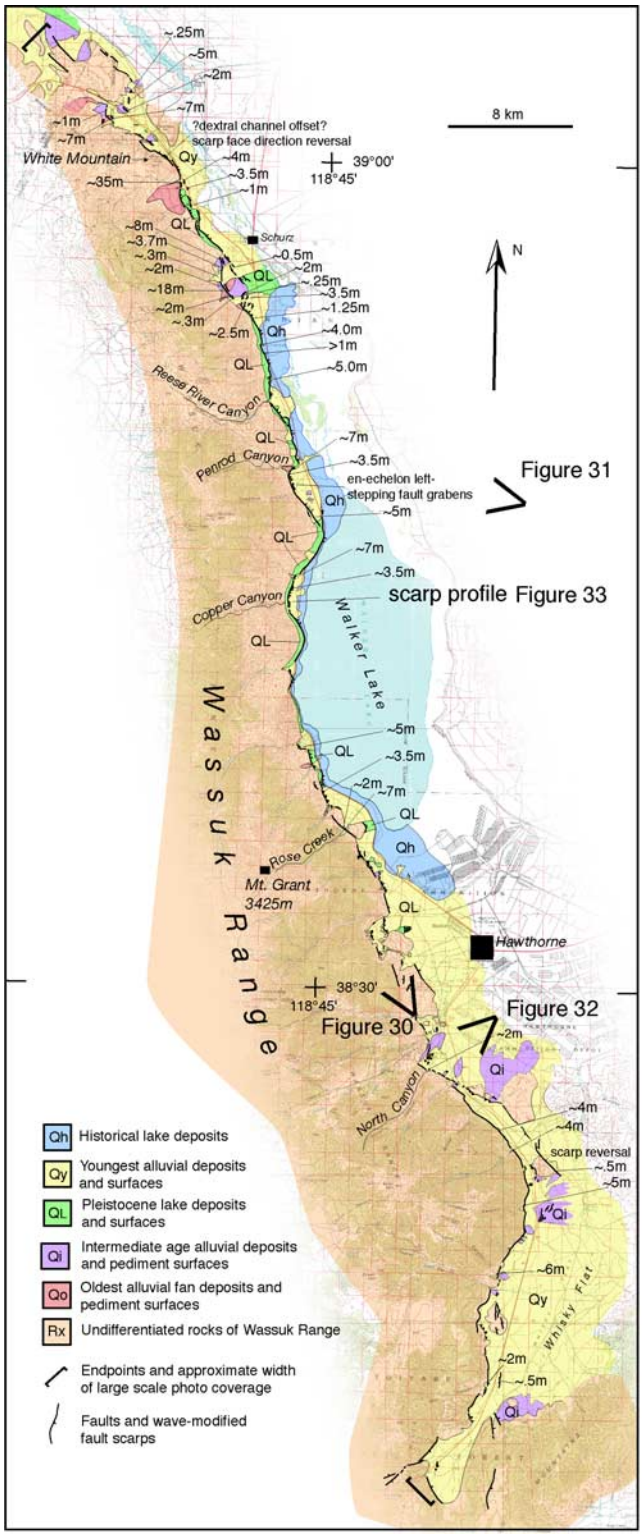

[36] The range front morphology and character of faulting along the Pilot Mountains differ from that observed along the Gabbs Valley Range to the north (Figure 18). The Pilot Mountains display an abrupt and steep escarpment, triangular facets, and a fault trace that primarily separates bedrock from alluvium. In contrast, faulting along the Gabbs Valley Range is commonly outboard of the range, the range front less steep, and triangular facets smaller. Elevations in the Pilot Mountains are also consistently higher, reaching >9000 feet (2800 m), in comparison to elevations of the Gabbs Valley Range which are generally less than 8000 feet (2500 m) (Figure 18). Scarps that cut young alluvium at the base of the Pilot Mountains are present north of about Water Canyon (Figure 19). At Mac Canyon, an alluvial scarp strikes into bedrock and a zone of fault gouge >10 m in thickness is present (Figure 19). The bedrock maps of *Oldow and Meinwald* [1992] and *Oldow and Dockery* [1993] show a linkage to the Bettles Wells fault (Figure 14). Scarps in young alluvium and the alignment of escarpments in older pediment surfaces to the northeast of Mac Canyon suggest that transfer of slip to the Bettles Wells and faults to the east may continue today (Figures 14 and 19), though the exact mechanics of the transfer are not clear. The transfer of slip is probably responsible for the difference in character of faulting and range front morphology observed between the two ranges. As well, the slightly more southerly strike of the Pilot Mountains section of the fault may result in a relatively increased normal component of displacement.

3.9. Gumdrop and Indian Head Faults

[37] The faults strike parallel to the Benton Springs fault (Figures 2 and 24). Geologic maps covering the region are many [*Dohrenwend*, 1982b; *Ekren and Byers*, 1984, 1985a, 1985b, 1986a, 1986b; *Hardyman*, 1978, 1980; *Stewart et al.*, 1982]. The Gumdrop fault strikes northwesterly ~55 km from Soda Springs Valley through the Gabbs Valley and Gillis Ranges. A Cretaceous granite is displaced 6.4 km right laterally near the northern extent of the fault within the Gillis Range (Figure 2) [*Hardyman*, 1978, 1980]. Sedimentary rocks of Triassic age intersect the fault at high angle and are offset about 9 km right laterally where the fault enters Soda Springs Valley (Figure 2) [*Ekren and Byers*, 1984]. Most of the offset is interpreted to predate 5.8 my [*Ekren*

Figure 29. Fault trace along Wassuk range front. Scarp heights are labeled in meters. Units Qy, Qi, and Qo are Quaternary surfaces of relatively increasing age. Lacustrine deposits exposed primarily during historical lake recession denoted Qh. Surfaces largely unmodified since recession of late Pleistocene Lake Lahontan are QL. Unit Rx is undifferentiated. See text for further discussion. Perspectives of photo in Figures 30, 31, and 32 are shown by open ended V shape.

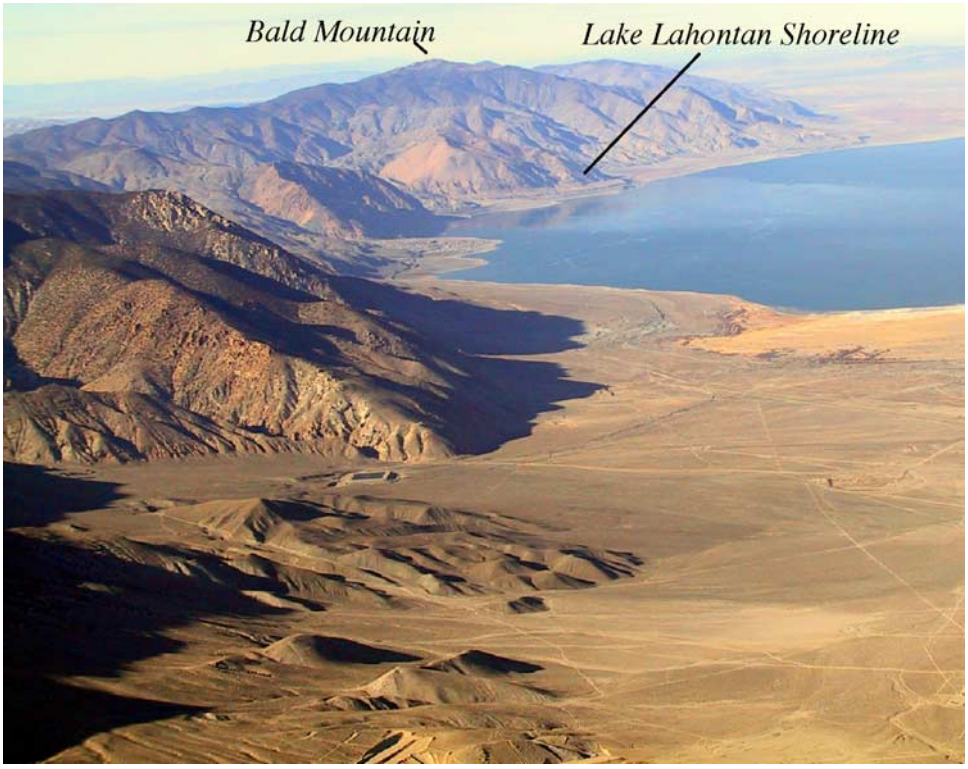

Figure 30. View north along Wassuk range front and Walker Lake from near North Canyon. Steep range front, triangular facets, and sinuous range front reflect active normal faulting. Perspective of photo is shown in Figure 29. Wave-cut benches and escarpments mark shoreline of pluvial Lake Lahontan along the base of the range front.

et al., 1980]. Linear fault-controlled valleys mark the trace of the fault as it extends northward from Soda Springs Valley to Win Wan Valley, where the fault bends or steps to the right and continues along the west flank of Chukar Ridge (Figure 24). Geomorphic features in Quaternary deposits and indicative of right-lateral displacement, albeit few, are present along the fault south of Nugent Wash (Figure 24). Dextral channel offsets on the order of ~10 m occur along the east side of Win Wan Flat (Figure 24). The most youthful expression of lateral displacement is preserved at the southern limit of the fault where deposits of late Pleistocene or Holocene age are offset dextrally about ~10 m (Figures 25 and 26).

[38] The Indian Head fault displaces late Pleistocene or Holocene deposits in Soda Springs Valley, forms a linear and abrupt range front as it strikes northwestward toward Indian Head Peak, then is marked by numerous shutter ridges and dextral stream deflections of 50–250 m in Paymaster Canyon (Figures 24 and 27). *Ekren and Byers* [1984] observe 4–5 km of right offset across the fault of a steeply dipping marker bed within the Triassic Luning formation (Figure 2). Triangular facets south of Indian Head Peak suggest an additional and significant component of vertical motion. Scarps in older elements of the active fan apron on the southwest flank of the Indian Head Peak ridge record the most recent and probable dextral displacement along the fault (Figure 28). A strand of the fault that cuts older gravel surfaces and parallels the Benton Springs fault north of Wildhorse Canyon may be a continuation of the fault, though younger surfaces southward toward Paymaster Canyon do not appear to be broken (Figure 24).

3.10. Wassuk Range

[39] The Wassuk Range is an east tilted fault block that strikes northwesterly about 50 miles (80 km), reaches elevations exceeding 3000 m, and is bounded on the east by a high-angle normal fault (Figures 2 and 29). Thermochronologic analysis suggests that much of an 8.5 km

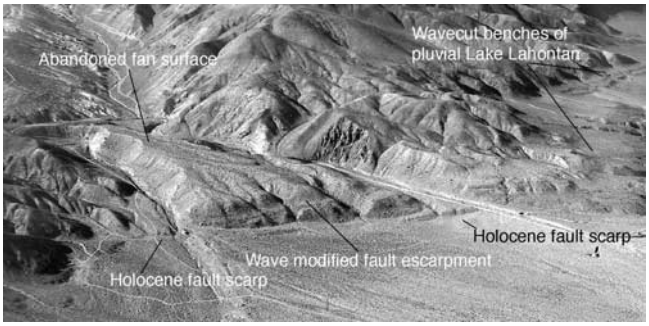

Figure 31. Older alluvial fan surface truncated by wave-modified fault scarp which records longer-term Quaternary uplift, and lesser scarps in younger washes which reflect most recent normal fault activity at Penrod Canyon. Perspective of photo is shown in Figure 29.

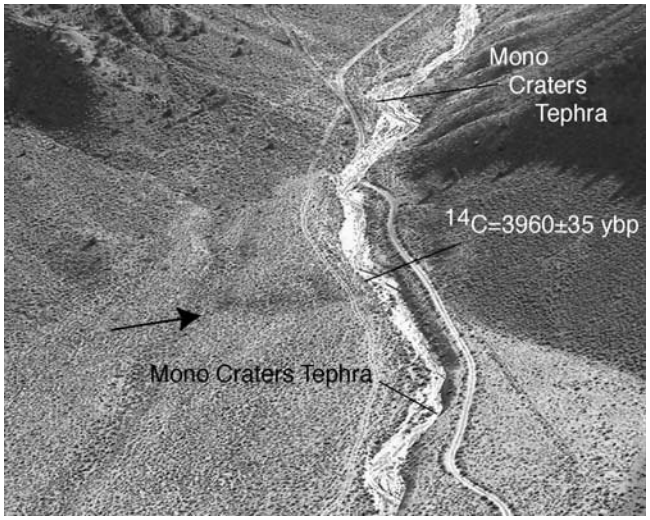

Figure 32. Arrow points to fault scarp at mouth of North Canyon. Radiocarbon from the footwall (sample NCRC-SGW) places formation of the scarp at <3960 ± 35 ^{14}C years B.P. Mono Craters tephra is found in both footwall (sample 081899-T3 in Table 2) and sediments deposited after the scarp formed on the hanging wall (sample NCT1-SGW in Table 2).

unroofing and uplift of the range occurred between ~15 and ~12 Ma, followed by a later period of extension concentrated along the east flank of the range ~4 Ma [*Stockli et al.*, 2002]. The steep east flank of the range exhibits the abrupt sinuous trace and triangular facets characteristic of an active normal fault (Figure 30). The deepest part of the adjoining basin is filled by Walker Lake. Walker Lake has dropped ~40 m in level since the turn of the century due to human water diversions and reached elevations of ~1330 m during late Pleistocene about 13 ka [e.g., *Adams and Wesnousky*, 1999]. Vestiges of the late Pleistocene highstand are visible as wave-cut benches and escarpments along the base of the range (Figures 30 and 31). Holocene scarps commonly reach 4 m to 6 m height and are present at the mouths of active washes along the entirety of the range front. Longer-term Quaternary offset is preserved in 20- to 40-m-high scarps truncating older alluvial fan surfaces near White Mountain, southwest of Schurz, and Penrod Canyon (Figure 29). The location of the lake adjacent to the range front reflects a continuous west tilting and subsidence of the hanging wall. Relationships at Penrod Canyon are representative of much of the range front (Figure 31). Active drainages are broken by Holocene scarps. The Holocene scarps strike parallel and immediately in front of a larger wave-modified escarpment that truncates an older Quaternary alluvial surface. The position of the Holocene scarps indicates the larger escarpment and the uplift of the older alluvial fan surface are largely tectonic in origin. Holocene scarps are generally simple in form suggesting a single-event origin [e.g., *Wallace*, 1977]. Charcoal taken from the footwall of a natural exposure at North Canyon (sample NCRC-SGW, Table 1) places a maximum bound on the age of the last earthquake at 3960 ± 35 ^{14}C years B.P. (Figures 29 and 32). Mono Craters tephra taken from unbroken deposits on the hanging wall (sample NCT1-SGW, Table 2) and deposits in the footwall (sample 081899-T3, Table 2) match best with late Holocene Mono Craters tephra ranging in age from ~800 to ~2000 ^{14}C years B.P., but conservatively may be as young as ~600 ^{14}C years B.P. or as old as ~6700 ^{14}C years B.P. (A. Sarna-Wojcicki, U.S. Geological Survey, Menlo Park, California, personal

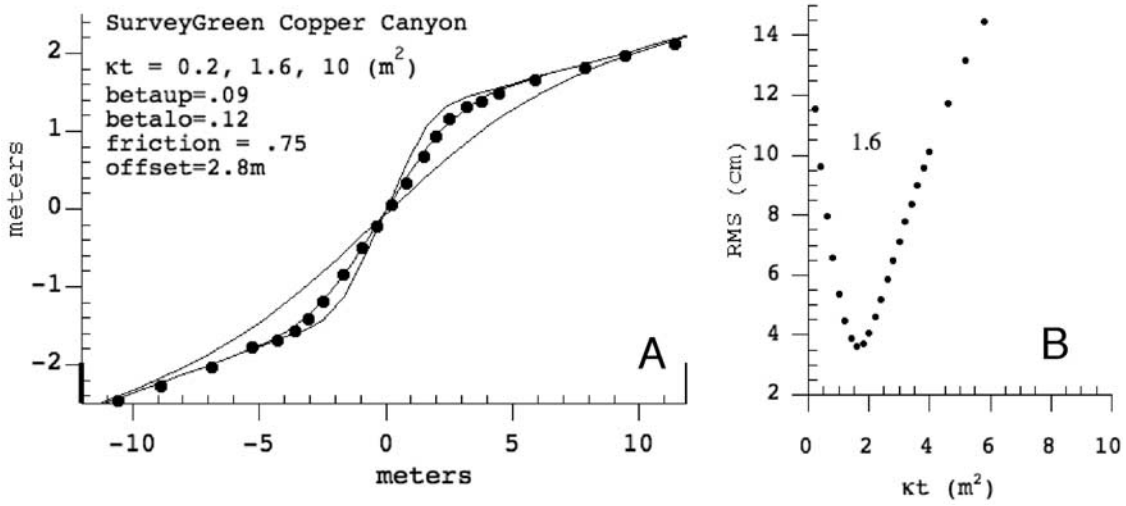

Figure 33. Analysis of scarp in young alluvium at Copper Canyon. (a) Measured (dots) and synthetic profile (lines) of scarp computed for values of κt listed and those that yield the best fit of the synthetic to the observed profile and two bounding values of κt. (b) Root-mean-square misfits of synthetic to observed profiles as a function of κt. The value κt = 1.6 resulting in the minimum misfit is listed and indicates a late Holocene offset when κ is assumed to equal 1.1. See Figure 10 for explanation of other variables.

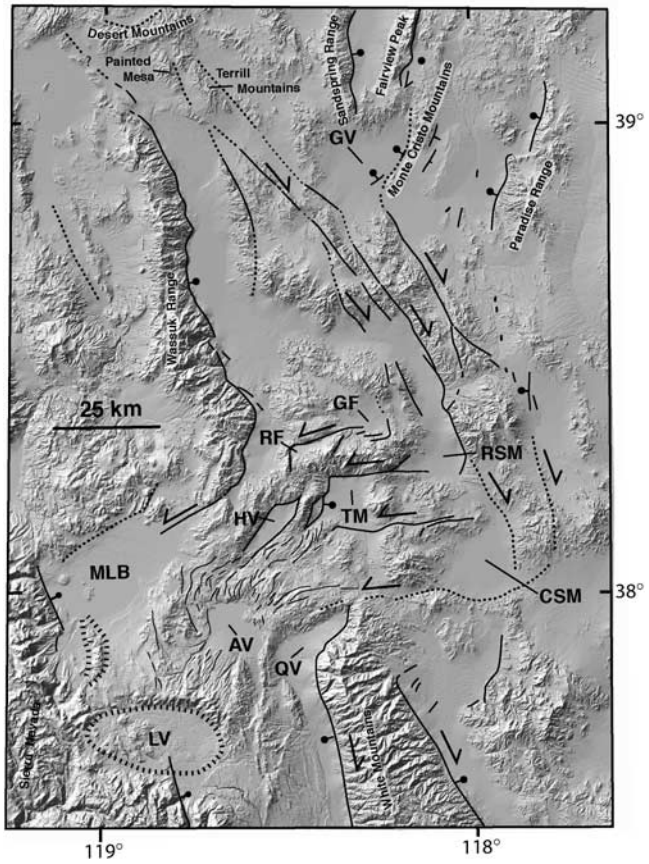

Figure 34. Active fault traces superimposed on digital relief model of central Walker Lane and surrounding areas. Locations of basins are annotated GV, Gabbs Valley; RF, Rattlesnake Flat; GF, Garfield Flat; RSM, Rhodes Salt Marsh; TM; Teels Marsh; HV, Huntoon Valley; MLB, Mono Lake Basin; AV, Adobe Valley; QV, Queen Valley; CSM, Columbus Salt Marsh; LV, Long Valley. Sense of strike slip and dip slip on active fault traces is shown by half-sided arrows and bar-and-ball on hanging wall, respectively.

communication, 2003). Synthetic modeling of a young scarp profile farther north at Copper Canyon (Figure 29), where both the footwall and hanging wall are unmodified by fluvial processes, shows the shape of the scarp is consistent with formation in the late Holocene (Figure 33). The dates and visual similarities in the profiles of young scarps along the range suggests that the entirety of the range front fault has ruptured in late Holocene time.

3.11. Synopsis of Observations

[40] The geomorphic expression of each of the faults is consistent with continuous Quaternary offset and most recent displacements are late Pleistocene and Holocene in age. Youthful displacements on the east striking Rattlesnake, Excelsior Mountains, Candelaria and, probably, the Anchorite Hills faults show the faults are primarily left lateral, whereas the northwest striking Petrified Springs, Benton Springs, Gumdrop, and Indian Head faults are right lateral. The Wassuk Range front in contrast is bound by an east dipping normal fault. Quantitative limits on the recency and rate of slip on the faults are less forthcoming. Radiocarbon and tephra samples collected from natural and excavated exposures place the age of last displacement along the Wassuk Range and Benton Springs faults at about 1000–4000 years B.P. and 780 ± 35 ^{14}C years B.P., respectively. Soil development on surfaces into which channels and channel banks are incised and offset by the Petrified Springs and Benton Hills faults are interpreted to place minimum slip rate values of ~1 mm/yr on each.

4. Discussion

[41] The distribution of fault traces in the central Walker Lane and the sense of slip for each are depicted in Figure 34. The east striking faults within the map area sit within a right step between northwest striking strike-slip faults of southern Walker Lane and the northern portion of the map area, respectively (Figures 1 and 34). Cumulative right-lateral offsets on northwest striking fault systems to the north and south of the right step are on the order of ~50 km or greater. *Oldow et al.* [1994] conclude that much of the mid-Miocene to Pliocene transfer of slip through the right step has been accomplished by displacement on an east trending shallow northwest dipping low-angle detachment fault system that has exposed the Silver Peak–Lone Mountain extensional complex (Figure 1). That is not the case today. Faulting and slip transfer through the step is occurring on steeply dipping left-lateral strike-slip faults which are conjugate and define an angle of ~70° with the northwest striking right-lateral faults. On the basis of the geometry, it is reasonable to infer the fault-bounded blocks are also undergoing a clockwise component of vertical axis rotation [*Freund*, 1974; *Nur et al.*, 1986; *Ron et al.*, 1984]. The mode of slip transfer is quite different to the south in the southern Walker Lane. There, steeply dipping and northeast striking normal faults transfer slip across a series of right steps from the northwest trending Owens Valley and Hunter Mountain fault systems to the Fish Lake Valley fault zone [*Lee et al.*, 2001a; *Oswald and Wesnousky*, 2002; *Reheis and Dixon*, 1996].

[42] The genesis of the current configuration of faults is problematic. The conjugate orientation cannot be explained by conventional Mohr-Coulomb faulting theory and laboratory-derived values of internal rock friction. The theory and observation predict that conjugate fault sets should trend about 25°–30° from the direction of maximum principal contraction (Figure 35a) [*Anderson*, 1951; *Byerly*, 1978; *Jaeger and Cook*, 1979], whereas here it is greater than 90° (Figure 34). Inherited structure may play a role in the development and current orientation of the east striking left-lateral faults. For example, the location and trend of left-lateral faults may coincide with the orientation of earlier Cenozoic structure and the edge of the continent as it existed in the Paleozoic [e.g., see *Oldow*, 1984; *Oldow et al.*, 1994; *Stewart*, 1985]. Another possibility arises from empirical fault models of simple shear. Such models, for right-lateral simple shear, show conjugate left-lateral

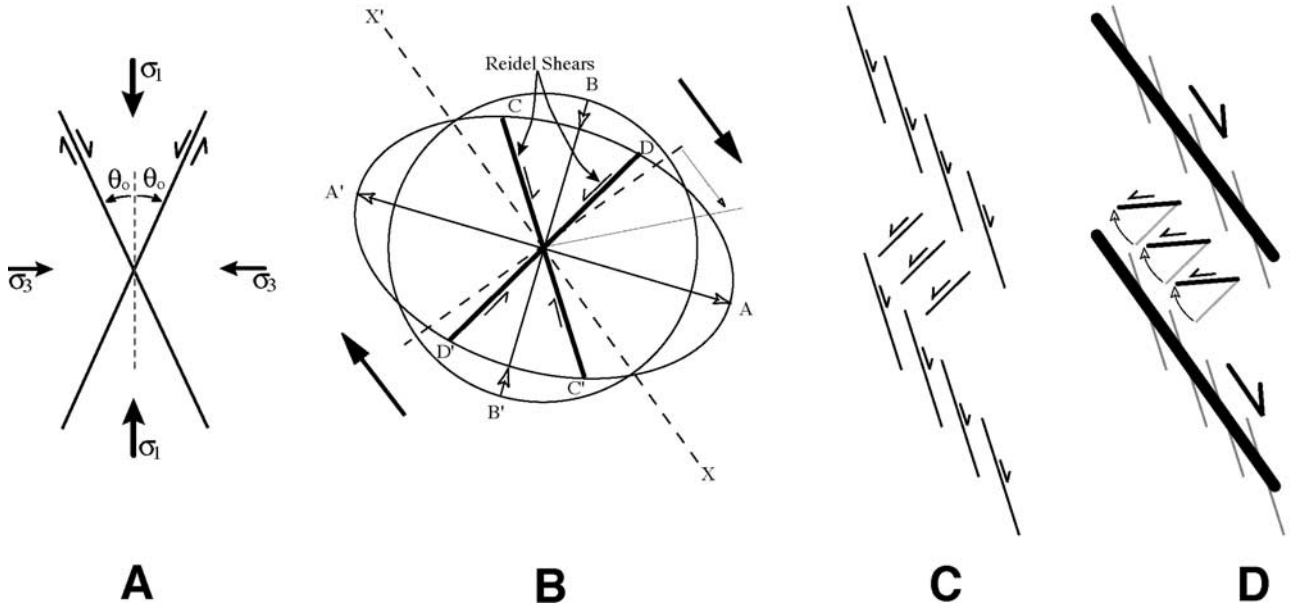

Figure 35. Elements of discussion concerning development of conjugate orientation of faults in the central Walker Lane. (a) Shear failure in rock subject to pure shear and assumption of standard values of fault friction ($\mu \sim 0.75$) predicting fault plane development at angles of about $\theta_O = 30°$ from the direction of maximum compression σ_1 [e.g., *Anderson*, 1951]. (b) Empirically observed orientation of failure planes (Reidel Shears) developed in laboratory models upon initiation of simple shear. Adapted from *Wilcox et al.* [1973] and rotated so shear is oriented approximately parallel to the Walker Lane. (c) Conceptualized inception of fault system due to simple shear characterized by en echelon right-slip faults along trend parallel to main zone of shear and conjugate left-slip faults in step-over between main zones of right shear. (d) Continued displacement results in coalescence of main shear zones (bold lines) and continued left slip and clockwise rotation of conjugate faults.

(Reidel) shears form at angles near perpendicular to the main shear direction (Figure 35b). The easterly striking left-lateral faults within the central Walker Lane may have originated as left-slip faults conjugate to the main zone of right-lateral shear and have since rotated 20°–30° clockwise into their current position (Figures 35c and 35d).

[43] Crustal blocks bounded by faults that are conjugate to a main zone of strike slip have been observed to progressively rotate on vertical axes with continued deformation [e.g., *Cashman and Fontaine*, 2000; *Freund*, 1974; *Garfunkel*, 1974; *Garfunkel and Ron*, 1985; *Luyendyk*, 1991; *Luyendyk et al.*, 1980; *Nicholson et al.*, 1986, 1994; *Ron et al.*, 1984]. It has also been shown that the amount of slip on conjugate faults that bound crustal blocks within zones of simple shear is related to the amount of rotation [*Freund*, 1974; *Ron et al.*, 1984]. For the special case that conjugate shears remain in contact with bounding right-lateral shear zones, the geometrical relation between the displacement d on the conjugate block-bounding faults, the width w of the faulted blocks, the initial angle α between the conjugate faults and the main boundary shear, and the angle of rotation δ (positive clockwise) is expressed as $d = w*(\sin\delta/(\sin\delta\sin(\alpha - \delta))$ [*Freund*, 1974; *Ron et al.*, 1984]. The width of crustal blocks bounded by the Rattlesnake, Excelsior, and Candelaria Fault zones is about 10 km. If we assume the faults were originally oriented about $\alpha = 90°$ to the northwest trending strike-slip faults of the central Walker Lane and rotated $\delta = 20°$ clockwise to their current orientation (e.g., Figures 35c and 35d), then $\alpha - \delta = 70°$, and the formula predicts left-lateral displacement of about 3 to 4 km on the block-bounding faults. The boundary conditions for the calculation do not take into account various volumetric considerations and the extensional component of deformation across the Walker Lane. That

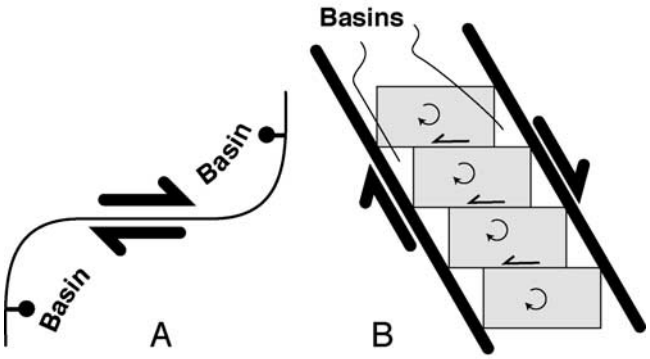

Figure 36. Pairing of basins at ends of east striking faults may be the result of (a) simple left-slip transform of motion between normal fault basins or (b) clockwise rotation of crustal blocks within northeast trending zone of right shear. Elements of both processes appear responsible for major basins within the central Walker Lane.

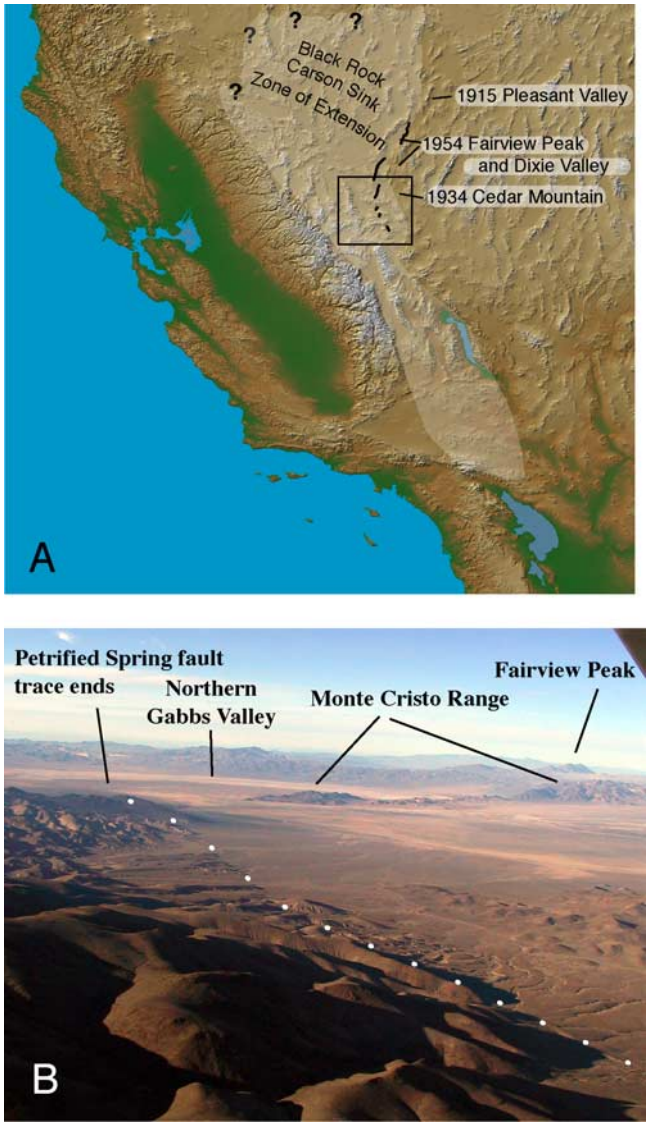

Figure 37. (a) Central Walker Lane (box) located where recent geodesy indicates a belt of high northwest directed right-lateral shear strain within the Mojave Desert and east of the Sierra Nevada (light overlay) widens to encompass the central Nevada Seismic Belt (CNSB) and Black Rock–Carson Sink Zone of Extension (BRCSZE). Queries emphasize uncertainty of boundaries to north. (b) Process of slip transfer from northwest trending strike-slip faults of the Walker Lane to northeasterly trending normal faults along the CNSB and in the BRCSZE is structurally and physiographically expressed in the intersection of the normal fault-bounded Fairview Peak and Monte Cristo Range with the abrupt end of the Petrified Springs strike-slip fault. View is northward.

withstanding, the exercise provides an idea of the magnitude of slip that might be expected on the left-slip faults. Paleomagnetics and identification of geologic piercing points might be used to test the idea.

[44] A consistent pairing of basins at the endpoints of each of the left-lateral east striking faults is evident in the digital elevation model of Figure 34. For example, Rattlesnake Flat and Garfield Flat are formed along the southwest and northeast ends of the Rattlesnake fault, respectively. Teels Marsh and Rhodes Salt Marsh have similarly developed at the ends of the Excelsior Mountain fault. The locations of the basins are that which would be expected from volumetric considerations at the ends of left-lateral strike-slip faults which transfer slip between normal-faulted basins (Figure 36a) or which have formed due to clockwise vertical axis rotation (Figure 36b). Given that the Walker Lane is transtensional [e.g., *Unruh et al.*, 2003], elements of both processes are likely embodied in the formation of the basins. Analogously, I infer that Columbus Salt Marsh and Queen Valley also result from accommodation of lateral slip and fault rotation on the Coaldale fault zone. Absence of basins at the ends of the Candelaria fault suggests that total slip along the fault is less.

[45] The northwestward extension and manner of termination of the major northwest striking faults of the central Walker Lane is enigmatic. Some insight arises by coupling recent geodetic observations with observations collected in this study. GPS analyses indicate the belt of high northwest directed right-lateral shear strain observed within the Mojave Desert and east of the Sierra Nevada widens at about the latitude of this study to also include portions of the western Basin and Range (Figure 37) [*Bennett et al.*, 2003; *Dixon et al.*, 2000, 1995; *Savage et al.*, 2001; *Thatcher et al.*, 1999]. The widening is also reflected in analyses of individual geodetic arrays that span the Walker Lane. Right-lateral shear across the Walker Lane is significantly less across the northern Walker Lane (6 ± 2 mm/yr) [*Thatcher et al.*, 1999] as compared to that measured across the latitude of this study ($\sim$10 mm/yr) [*Oldow et al.*, 2001] and southward in the southern Walker Lane (11 ± 1 mm/yr) [*Dixon et al.*, 2000, 1995]. The observations suggest that, at or just to the north of the latitude of the central Walker Lane, a significant component of Walker Lane strike slip is being transferred to normal faults and northwest directed extension in the Basin and Range (Figure 37).

[46] The Petrified Springs fault is well expressed geomorphically and characterized by a right-slip rate of $>\sim$1 mm/yr. Yet, the fault abruptly terminates as it reaches Gabbs Valley and the southward extent of the Monte Cristo Range (Figure 37). I surmise the abrupt termination represents transform of strike slip to dip slip along the Monte Cristo Range and Fairview Peak to the northeast which, in effect, may also be largely responsible for the formation of northern Gabbs Valley. The 1932 Cedar Mountain ruptures also extend north into the Monte Cristo Mountains and appear to represent a transfer or leakage of northwest directed right-lateral shear to northeast striking normal faults of the Basin and Range [*Bell et al.*, 1999]. It is this process which accounts for the widening of the strain field and the lesser rates of geodetically measured strike slip in the northern Walker Lane as compared to the southern Walker Lane.

[47] The geomorphic expression of the Gumdrop, Benton Springs, and Wassuk faults decreases to the north of the

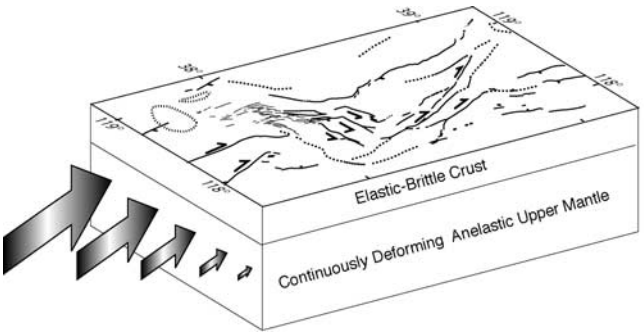

Figure 38. Complexity of faulting and apparent rotation of crustal blocks in the central Walker Lane suggesting an elastic brittle crust in part detached and riding on underlying zone of continuous shear. Orientation and increasing size of arrows schematically depict direction and sense of right-lateral shear across the central Walker Lane.

regions covered in Figures 19, 24, and 29, respectively. The linear and sharp east flanks of the Terrill Mountains and Painted Mesa may be the continuation of the Gumdrop and Benton Springs fault systems (Figure 34). Similarly, an alignment of bedrock knobs extends northwest from the Wassuk Range and probably defines the northwest continuation of the range-bounding fault, possibly with a component of strike slip due to its more westerly strike (Figure 34). Each of the northwest trending faults appears to end abruptly against the east trending Desert Mountains. The apparent decrease in geomorphic expression and the abrupt termination of the faults at the Desert Mountains probably reflects both the transformation of northwest directed strike slip into the rotation of crustal blocks within the Carson Block [e.g., *Cashman and Fontaine*, 2000] (Figure 1) as well as to normal displacement in the western Basin and Range.

[48] The northward decrease in the rate of shear across the Walker Lane suggested in recent geodesy may be mimicked by a decrease in cumulative right slip along the Walker Lane. Available observations are coupled with significant uncertainty but nonetheless suggest that cumulative right offset decreases from upward of 65–100 km in the Eastern California Shear Zone and southern Walker Lane [*Dokka and Travis*, 1990a; *Stewart*, 1988] to 48–60 km in the central Walker Lane [*Ekren and Byers*, 1984; *Ekren et al.*, 1980; *Hardyman*, 1984] and a possible 32 km in the northern Walker Lane [*Bonham*, 1969; *Faulds et al.*, 2003; *Stewart*, 1988]. The apparent shared northward decrease in strain rate and cumulative offset allows the suggestion that the currently observed pattern of shear strain accumulation is characteristic of the long-term deformation field as well. That the geodetically observed widening of the deformation field may be correlated to clear physiographic expression of slip transfer from the Walker Lane to the Basin and Range as observed at the north end of the Petrified Springs fault (Figure 37) supports the idea. A relationship of the geodetically observed strain field to geologic features observed over the longer term is also embodied in the work of *Wallace* [1984]. He defined a "Black Rock–Carson Sink Zone of Extension" tectonic subprovince (Figure 37). The province spatially mimics the geodetically observed widening of the Walker Lane zone of shear into the western Basin and Range. The subprovince is distinguished by especially broad alluviated grabens separated by bedrock horsts and interpreted by *Wallace* [1984] to suggest that this zone has been an area of greater, possibly more rapid extension than surrounding areas during late Tertiary time and that relatively greater thinning of the upper crust has occurred.

[49] Observations of the complex patterns of faulting in the Basin and Range led *Wallace* [1978b] to propose that faulting occurs in a weak, previously fractured and brittle crust in response to an underlying zone of anelastic defor-

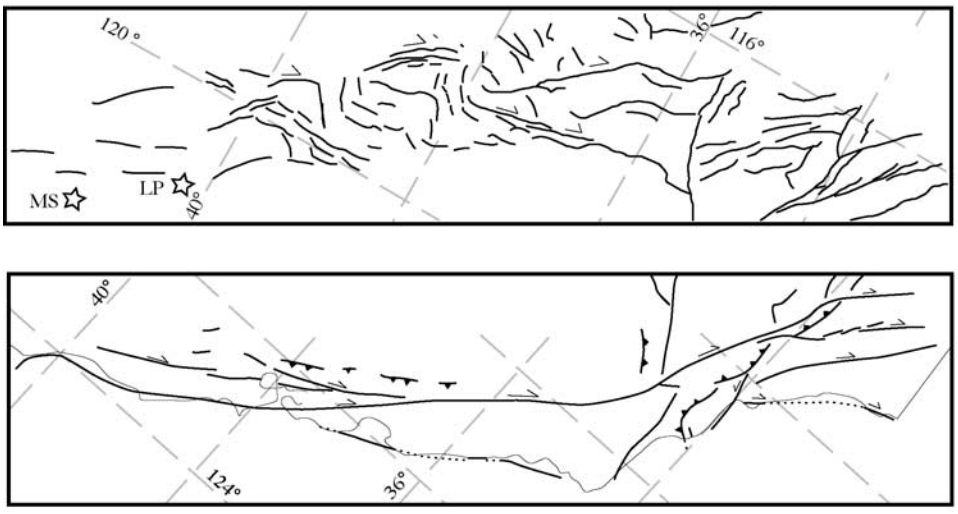

Figure 39. Pattern of fault traces along (bottom) the San Andreas fault system is simpler than observed within (top) the Walker Lane. Maps are plotted to same scale and rotated for convenience of comparison. Lassen Peak (LP) and Mount Shasta (MS) volcanoes marked by stars.

mation. *Jackson and Molnar* [1990] similarly pointed to active rotation of crustal blocks in California to interpret that blocks of continental crust are carried by a continuously deforming substratum. The complexity of faulting and apparent rotation of crustal blocks within the central Walker Lane are consistent with the idea of a partially detached elastic-brittle crust that is being transported on an underlying zone of continuous shear (Figure 38).

[50] Although the strike-slip systems of the Walker Lane and San Andreas take up the largest share of Pacific–North American transform plate motion, the pattern of faulting displayed by each is significantly different (Figure 39). The pattern of faulting along the San Andreas is dominated by the relatively smooth and continuous trace of the San Andreas fault. Other subsidiary strike-slip strands such as the San Jacinto and Hayward-Maacama fault systems are essentially interconnected, branching off at small angles to the San Andreas fault. In contrast, there exists no single throughgoing strand along the Walker Lane. Northwest trending strike-slip faults that define the shear zone are discontinuous and interrupted by zones of east trending left-lateral faults. Faults composing the Walker Lane define a broader and more diffuse pattern than the San Andreas system.

[51] The more complex, diffuse, and discontinuous nature of the faults defining the Walker Lane and Eastern California Shear Zone as compared to the San Andreas system may largely be due to differences in the cumulative geologic slip taken up by each [*Wesnousky*, 2005]. Measures of cumulative right slip on active strands of the San Andreas system range from about 300 to 450 km [e.g., *Dillon and Ehlig*, 1993; *James et al.*, 1993], whereas cumulative slip across the Walker Lane is generally well less than 100 km. Laboratory studies suggest that strike-slip fault systems should be characterized by a zone of discrete fault segments during initial stages of development which ultimately coalesce to take up displacement along a principal and throughgoing fault [e.g., *Wilcox et al.*, 1973]. Field observations along individual strike-slip faults support the idea [*Stirling et al.*, 1996; *Wesnousky*, 1988]. In this case, the San Andreas fault system would be considered to be at a more mature stage of structural development than the Walker Lane.

[52] Another factor that may also play a role in yielding a more complex pattern of faulting in the Walker Lane fault is the attendant component of extension across the system [*Bennett et al.*, 2003]. The pattern of faulting observed to the west in the Basin and Range suggests a tendency for continental extension to be diffuse over broad areas. The component of extension transverse to the trend of the Walker Lane may also work against the coalescence and simplification of strike-slip deformation with continued offset [*Wesnousky*, 2005].

[53] Despite first-order differences in the gross pattern of faulting, important characteristics of deformation style are also shared by the San Andreas and Walker Lane systems. A feature shared by each system is accommodation of the oblique component of displacement on dip-slip faults that strike nearly parallel to the major strike-slip faults. The phenomenon, first recognized by *Fitch* [1972] along major subduction zones, has been discussed in some detail along the San Andreas [*Jones and Wesnousky*, 1992] and in the western Basin and Range [*Wesnousky and Jones*, 1994]. An example of this behavior along the San Andreas system is the occurrence of the 1980 *M*6.7 Coalinga thrust and associated folds which strike parallel to the adjacent central San Andreas fault [*Jones and Wesnousky*, 1992]. In like manner, the strike-slip trace of the 1872 $M \sim 7.9$ Owens Valley earthquake runs parallel to the adjacent Sierra Nevada range front normal fault [*Wesnousky and Jones*, 1994]. The behavior is also manifest in the parallel juxtaposition of the Wassuk Range front normal fault with the strike-slip faults of the central Walker Lane (Figures 2 and 34). Another similarity is expressed in the presence and attendant clockwise rotation of faults and fault blocks bounded by conjugate east striking left-slip faults in the central Walker Lane. Conjugate left-lateral faulting and clockwise rotation of crustal blocks is also a characteristic deformation style along the southern San Andreas fault system [e.g., *Luyendyk*, 1991; *Luyendyk et al.*, 1980; *Nicholson et al.*, 1986]. The clockwise rotation of crustal blocks has led to the development of structural basins along both fault systems. Also finally, it appears that much of the basin development along the San Andreas occurred during earlier stages of its evolution when it was transtensional like the Walker Lane today [*Luyendyk*, 1991; *Wesnousky*, 2005].

5. Conclusions

[54] Listed here in the order of development are the principal observations and inferences I have drawn from the field study.

[55] 1. The Petrified Springs and Bentons Springs faults take up the major portion of right-lateral plate motion at their latitude. The rate of right-lateral slip on each is at minimum $\sim$1 mm/yr during late Pleistocene.

[56] 2. The last surface rupture earthquakes along the Benton Springs fault and the Wassuk Range front fault occurred about 800 and subsequent to $\sim$4000 ^{14}C years B.P., respectively.

[57] 3. Slip transfer from the southern Walker Lane to the northern half of the central Walker Lane is being accommodated by rotation of crustal blocks bounded by steeply dipping east striking left-slip faults.

[58] 4. Major basins in the region, including Rattlesnake and Garfield flats, Teels, Columbus and Rhodes salt marshes, and Queen Valley, are principally the result of east trending left-slip faults and clockwise rotation of the crustal blocks they bound.

[59] 5. The abrupt northern limit of northwest trending strike-slip faults of the central Walker Lane is due to (1) transfer of right slip to dip slip on northerly striking range fronts of the central Nevada Seismic Belt (e.g., Petrified Springs fault) and (2) transformation of right slip to rotation of crustal blocks within the Carson Block to the north (e.g., Gumdrop and Benton Springs faults).

[60] 6. The transfer of right slip in the central Walker Lane to dip slip and extension in the western Basin and Range correlates to a northward broadening of the modern strain field and appears to be a long-lived feature of the deformation field.

[61] 7. The complexity of faulting and apparent rotation of crustal blocks within the Walker Lane are consistent with the concept of a partially detached elastic-brittle crust that is being transported on a continuously deforming anelastic substratum.

[62] 8. The more complex pattern of faulting observed along the Walker Lane as compared to the San Andreas system is due to the relatively smaller accumulation of right slip across the Walker Lane, and that the Walker Lane is characterized by a component of extension transverse to the principal direction of shear.

[63] 9. Characteristics of deformation style shared by the Walker Lane and San Andreas fault systems include clockwise rotations of crustal blocks bounded by faults conjugate to the main zone of shear, the development of structural basins due to the block rotations, and the partitioning of oblique components of slip onto subparallel strike-slip and dip-slip faults.

[64] **Acknowledgments.** Dick Hardyman introduced me to this area some 10 years ago, and I thank him for that. The final manuscript particularly benefited from the detailed review comments of Marith Reheis. I also thank Eric Kirby, Jeff Lee, and Bruce Luyendyk for their constructive comments. Andrei Sarna-Wojcicki, Elmira Wan, James Walker, Michelle Dodge, and Kristin Hepper at the USGS Tephrochronology Lab kindly identified volcanic ashes. Richard Briggs and Andrew Barron assisted me in excavation of soil pits and collection of scarp profiles along the Benton Springs and Excelsior faults. Thanks go to Geoff King, Yan Klinger, and James Dolan for input during a field visit to the area. I thank Kelvin Berryman, Mark Stirling, and Terry Webb for hosting me and use of facilities at Institute of Geological and Nuclear Sciences in New Zealand during the final stages of manuscript preparation. Editing was once Free. This material is based upon work supported by the National Science Foundation under grant EAR-0001006. Center for Neotectonic Studies contribution 43.

References

Adams, K. D., and S. G. Wesnousky (1999), The Lake Lahontan highstand: Age, surficial characteristics, soil development, and regional shoreline correlation, *Geomorphology*, *30*, 357–392.

Anderson, E. M. (1951), *The Dynamics of Faulting*, 206 pp., Oliver and Boyd, White Plains, N. Y.

Anderson, L. W., and F. F. Hawkins (1984), Recurrent Holocene strike-slip faulting, Pyramid Lake fault zone, *Geology*, *12*, 681–684.

Beanland, S., and M. Clark (1994), The Owens Valley fault zone, eastern California, and surface rupture associated with the 1872 earthquake, *U.S. Geol. Surv. Bull.*, *1982*, 1–29.

Bell, E. J. (1984), Overview of late Cenozoic tectonics of the Walker Lane, in *Western Geological Excursions*, *Guidebook*, vol. 4, edited by J. Lintz Jr., pp. 388–402, Geol. Soc. of Am., Boulder, Colo.

Bell, J. W. (1995), Quaternary geologic map of the Mina quadrangle, Nevada, *Nev. Bur. Mines Geol. Field Stud. Map, 10*, scale 1:24,000.

Bell, J. W., C. M. dePolo, A. R. Ramelli, A. M. Sarna-Wojcicki, and C. E. Meyer (1999), Surface faulting and paleoseismic history of the 1932 Cedar Mountain earthquake area, west-central Nevada, and implications for modern tectonics in the Walker Lane, *Geol. Soc. Am. Bull.*, *111*, 791–907.

Bennett, R. A., B. P. Wernicke, and J. L. Davis (1998), Continuous GPS measurements of contemporary deformation across the northern Basin and Range province, *Geophys. Res. Lett.*, *25*, 563–566.

Bennett, R. A., B. P. Wernicke, N. A. Niemi, A. M. Friederich, and J. L. Davis (2003), Contemporary strain rates in the northern Basin and Range province from GPS data, *Tectonics*, *22*(2), 1008, doi:10.1029/2001TC001355.

Billingsley, P., and A. Locke (1941), Structure of ore districts in the continental framework, *Trans. Am. Inst. Min. Metall. Eng.*, *144*, 9–59.

Birkeland, P. (1999), *Soils and Geomorphology*, 432 pp., Oxford Univ. Press, New York.

Bonham, H. F. (1969), Geology and mineral deposits of Washoe and Storey counties, Nevada, *Nev. Bur. Mines Geol. Bull.*, *70*, 1–140.

Briggs, R. W., and S. G. Wesnousky (2001), Paleoseismic evidence for repeated Holocene earthquakes on the Olinghouse fault zone, western Nevada, *Eos Trans. AGU*, *82*(47), Fall Meet. Suppl., Abstract S52D-0678.

Briggs, R. W., and S. G. Wesnousky (2004), Late Pleistocene fault slip rate, earthquake recurrence, and recency of slip along the Pyramid Lake fault zone, northern Walker Lane, United States, *J. Geophys. Res.*, *109*, B08402, doi:10.1029/2003JB002717.

Bucknam, R. C. (1974), Rattlesnake Flat-Whisky Flat area, in *Administrative Report: Progress Report on the Work Being Done in Support of Fault-Control Experiments to Be Conducted in the Nevada-California Seismic Zone*, edited by P. P. Orkild, pp. 8–13, U.S. Geol. Surv., Denver, Colo.

Bucknam, R. C., and R. E. Anderson (1979), Estimation of fault-scarp ages from a scarp-height-slope-angle relationship, *Geology*, *7*, 11–14.

Bull, W. B. (1991), *Geomorphic Responses to Climatic Change*, 326 pp., Oxford Univ. Press, New York.

Burchfiel, B. C., K. V. Hodges, and L. H. Royden (1987), Geology of the Panamint Valley-Saline Valley pull apart system, California: Palinspastic evidence for low angle geometry of a Neogene range-bounding fault, *J. Geophys. Res.*, *92*, 10,422–10,426.

Bursik, M., and K. Sieh (1989), Range front faulting and volcanism in the Mono Basin, eastern California, *J. Geophys. Res.*, *94*, 15,587–15,609.

Byerly, J. D. (1978), Friction of rocks, *Pure Appl. Geophys.*, *116*, 615–626.

Callaghan, E., and V. P. Gianella (1935), The earthquake of January 30, 1934 at Excelsior Mountains, Nevada, *Bull. Seismol. Soc. Am.*, *25*, 161–168.

Carlson, J. E., J. H. Stewart, D. C. Johannesen, and F. J. Kleinhampl (1978), Geologic map of the Walker Lake 1° by 2° quadrangle, Nevada-California, *U.S. Geol. Surv. Open File Rep.*, *78-253*, scale 1:250,000.

Carr, W. J. (1984), Regional structural setting of Yucca Mountain, southwestern Nevada, and Late Cenozoic rates of tectonic activity in part of the southwestern Great Basin, Nevada and California, *U.S. Geol. Surv. Open File Rep.*, *84-854*, 109 pp.

Cashman, P. H., and S. A. Fontaine (2000), Strain partitioning in the northern Walker Lane, western Nevada and northeastern California, *Tectonophysics*, *326*, 111–130.

Caskey, S. J., S. G. Wesnousky, and P. Zhang (1996), Surface faulting of the 1954 Fairview Peak (M_s = 7.2) and Dixie Valley (M_s = 6.8) earthquakes, central Nevada, *Bull. Seismol. Soc. Am.*, *86*, 761–787.

Crowell, J. C. (1974), Origin of late Cenozoic basins in southern California, in *Tectonics and Sedimentation*, edited by W. Dickinson, pp. 112–130, Soc. for Sediment. Geol., Tulsa, Okla.

Davis, G. A., and B. C. Burchfiel (1973), Garlock Fault: An intracontinental transform structure, southern California, *Geol. Soc. Am. Bull.*, *84*, 1407–1422.

DeMets, C., and T. H. Dixon (1999), New kinematic models for Pacific-North America motion from 3 Ma to present, I: Evidence for steady motion and biases in the NUVEL-1A model, *Geophys. Res. Lett.*, *26*, 1921–1924.

dePolo, C. M. (1989), Seismotectonics of the White Mountains fault system, east-central California and west-central Nevada, Master's thesis, Mackay Sch. of Mines, Univ. of Nev. Reno, Reno.

dePolo, C. M. (1993), Contemporary tectonics, seismicity, and potential earthquake sources in the White Mountains seismic gap, west-central Nevada and east-central California, USA, *Tectonophysics*, *225*, 271–299.

Dillon, J. T., and P. L. Ehlig (1993), Displacement on the southern San Andreas fault, in *The San Andreas Fault System: Displacement, Palinspastic Reconstruction, and Geologic Evolution*, edited by R. E. Powell, R. J. I. Weldon, and J. C. Matti, pp. 199–216, Geol. Soc. of Am., Boulder, Colo.

Dixon, T. H., S. Robaudo, J. Lee, and M. C. Reheis (1995), Constraints on present-day Basin and Range deformation from space geodesy, *Tectonics*, *14*, 755–772.

Dixon, T. H., M. Miller, F. Farina, H. Wang, and D. Johnson (2000), Present-day motion of the Sierra Nevada block and some tectonic implications for the Basin and Range province, North American Cordillera, *Tectonics*, *19*, 1–24.

Dohrenwend, J. C. (1982a), Preliminary surficial geologic map of the Excelsior Mountains area, west-central Nevada, *U.S. Geol. Surv. Misc. Field Stud. Map, MF-1372*, scale 1:62,500.

Dohrenwend, J. C. (1982b), Reconnaissance surficial geologic map of the Gabbs-Luning area, west-central Nevada, *U.S. Geol. Surv. Misc. Field Stud. Map, MF-1374*, scale 1:62,300.

Dokka, R. K. (1983), Displacements on late Cenozoic strike-slip faults of the central Mojave Desert, California, *Geology*, *11*, 305–308.

Dokka, R. K., and C. J. Travis (1990a), Late Cenozoic strike-slip faulting in the Mojave Desert, California, *Tectonics*, *9*, 311–340.

Dokka, R. K., and C. J. Travis (1990b), Role of the eastern California shear zone in accommodating Pacific-North American plate motion, *Geophys. Res. Lett.*, *17*, 1323–1326.

Doser, D. (1988), Source parameters of earthquakes in the Nevada seismic zone, 1915–1943, *J. Geophys. Res.*, *93*, 15,001–15,015.

Ekren, E. B., and F. M. Byers Jr. (1984), The Gabbs Valley Range—A well-exposed segment of the Walker Lane in west-central Nevada, in *Western Geological Excursions*, *Guidebook*, vol. 4, edited by J. Lintz Jr., pp. 203–215, Geol. Soc. of Am., Boulder, Colo.

Ekren, E. B., and F. M. Byers Jr. (1985a), Geologic map of the Gabbs Mountain, Mount Ferguson, Luning, and Sunrise Fault quadrangles, Mineral and Nye counties, Nevada, *U.S. Geol. Surv. Map, I-1577*.

Ekren, E. B., and F. M. Byers Jr. (1985b), Geologic map of the Win Wan Flat, Kinkaid NW, Kinkaid, and Indian Head Peak quadrangles, Mineral County, Nevada, *U.S. Geol. Surv. Map, I-1578*.

Ekren, E. B., and F. M. Byers Jr. (1986a), Geologic map of the Mount Annie NE, Mount Annie, Ramsey Spring, and Mount Annie SE quadrangles, Mineral and Nye counties, Nevada, *U.S. Geol. Surv. Map, I-1579*.

Ekren, E. B., and F. M. Byers Jr. (1986b), Geologic map of the Murphys Well, Pilot Cone, Copper Mountain, and Poinsettia Spring quadrangles, Mineral County, Nevada, *U.S. Geol. Surv. Map, I-1576*.

Ekren, E. B., R. C. Bucknam, W. J. Carr, D. G. L., and W. D. Quinlivan (1976), East trending structural lineaments in central Nevada, *U.S. Geol. Surv. Prof. Pap.*, *986*, 1–16.

Ekren, E. B., F. M. Byers Jr., R. F. Hardyman, R. F. Marvin, and M. L. Silberman (1980), Stratigraphy, preliminary petrology, and some structural features of Tertiary volcanic rocks in the Gabbs Valley and Gillis Ranges, *U.S. Geol. Surv. Bull.*, *1464*, 1–54.

Faulds, J. E., C. D. Henry, and N. H. Hinz (2003), Kinematics and cumulative displacement across the northern Walker Lane, an incipient transform fault, northwest Nevada and northeast California, *Geol. Soc. Am. Abstr. Programs*, *35*(6), 305.

Ferguson, H. G., and S. W. Muller (1949), Structural geology of the Hawthorne and Tonopah quadrangles, Nevada, *U.S. Geol. Surv. Prof. Pap.*, *216*, 55 pp.

Fitch, T. J. (1972), Plate convergence, transcurrent faults and internal deformation adjacent to Southeast Asia and the western Pacific, *J. Geophys. Res.*, *77*, 4432–4460.

Freund, R. (1974), Kinematics of transform and transcurrent faults, *Tectonophysics*, *21*, 93–134.

Gan, W. J., J. L. Svarc, J. C. Savage, and W. H. Prescott (2000), Strain accumulation across the Eastern California Shear Zone at latitude 36°30′N, *J. Geophys. Res.*, *105*, 16,229–16,236.

Garfunkel, Z. (1974), Model for the late Cenozoic tectonic history of the Mojave Desert, *Geol. Soc. Am. Bull.*, *85*, 1931–1944.

Garfunkel, Z., and H. Ron (1985), Block rotation and deformation by strike-slip faults: 2. The properties of a type of macroscopic discontinuous deformation, *J. Geophys. Res.*, *90*, 8589–8602.

Garside, L. J. (1982), Geologic map of the Moho Mountain quadrangle, Nevada, *Nev. Bur. Mines Geol. Map, 74*, scale 1:24,000.

Gianella, V. P., and E. Callaghan (1934), The earthquake of December 20, 1932, at Cedar Mountain, Nevada and its bearing on the genesis of Basin and Range structure, *J. Geol.*, *47*, 1–22.

Gilbert, C. M., N. M. Christensen, Y. Al-Rawii, and K. R. Lajoie (1968), Structural and volcanic history of Mono Basin, California-Nevada, *Mem. Geol. Soc. Am.*, *116*, 275–329.

Gillespie, A. R. (1982), Quaternary glaciation and tectonics in the southeastern Sierra Nevada, Inyo County, California, Ph.D. thesis, 695 pp., Calif. Inst. of Technol., Pasadena.

Goter, S. K., D. H. Oppenheimer, J. J. Mori, J. C. Savage, and R. P. Masse (1994), Earthquakes in California and Nevada, *U.S. Geol. Surv. Open File Rep., 94-647*.

Hanks, T. C., and D. J. Andrews (1989), Effect of far-field slope on morphologic dating of scarplike landforms, *J. Geophys. Res.*, *94*, 565–573.

Hanks, T. C., and R. E. Wallace (1985), Morphological analysis of the Lake Lahontan shoreline and beach-front fault scarps, Pershing County, Nevada, *Bull. Seismol. Soc. Am.*, *75*, 835–846.

Harden, J. W. (1982), A quantitative index of soil development from field descriptions: Examples from a chronosequence in central California, *Geoderma*, *28*, 1–23.

Hardyman, R. F. (1978), Volcanic stratigraphy and structural geology of the Gillis Canyon quadrangle, northern Gillis Range, Mineral County, Nevada, Ph.D. thesis, Univ. of Nev., Reno.

Hardyman, R. F. (1980), Geologic map of the Gillis Canyon quadrangle, Mineral County, Nevada, *U.S. Geol. Surv. Map, I-1237*.

Hardyman, R. F. (1984), Strike-slip, normal, and detachment faults in the northern Gillis Range, Walker Lane of west-central Nevada, in *Western Geological Excursions*, *Guidebook*, vol. 4, edited by J. Lintz Jr., pp. 184–199, Geol. Soc. of Am., Boulder, Colo.

Hardyman, R. F., and J. S. Oldow (1991), Tertiary tectonic framework and Cenozoic history of the central Walker Lane, Nevada, in *Geology and Ore Deposits of the Great Basin*, edited by G. L. Raines, pp. 279–302, Geol. Soc. of Nev., Reno.

Jackson, J., and P. Molnar (1990), Active faulting and block rotations in the western Transverse Ranges, California, *J. Geophys. Res.*, *95*, 2073–2087.

Jaeger, J. G., and N. G. W. Cook (1979), *Fundamentals of Rock Mechanics*, 585 pp., CRC Press, Boca Raton, Fla.

James, E. W., D. L. Kimbrough, and J. M. Mattinson (1993), Evaluation of displacements of pre-Tertiary rocks on the northern San Andreas fault using U-Pb zircon dating, initial SR, and common Pb isotopic ratios, in *The San Andreas Fault System: Displacement, Palinspastic Reconstruction, and Geologic Evolution*, edited by R. E. Powell, R. J. I. Weldon, and J. C. Matti, *Mem. Geol. Soc. Am.*, *178*, 257–271.

Jennings, C. W. (1994), Fault activity map of California and adjacent lands, Calif. Div. of Mines and Geol., Sacramento.

Jones, C. H., and S. G. Wesnousky (1992), Variation in strength and slip rate along the San Andreas fault system, *Science*, *256*, 83–86.

Klinger, R. E. (2001), Evidence for large dextral offset near Red Wall Canyon, in *Quaternary and Late Pliocene Geology of the Death Valley Region: Recent Observations on Tectonics, Stratigraphy, and Lake Cycles*, edited by M. N. Machette, M. L. Johnson, and J. Slate, *U.S. Geol. Surv. Open File Rep., 01-51*, A32–A37.

Kylander-Clark, R. C., D. S. Coleman, A. F. Glazner, and J. M. Bartley (2005), Evidence for 65 km of dextral slip across Owens Valley, California, *Geol. Soc. Am. Bull.*, *117*, 962–968.

Lee, J., C. Rubin, and A. Calvert (2001a), Quaternary faulting history along the Deep Springs Fault, California, *Geol. Soc. Am. Bull.*, *113*, 855–869.

Lee, J., J. Spencer, and L. Owen (2001b), Holocene slip rates along the Owens Valley Fault, California; Implications for the recent evolution of the Eastern California Shear Zone, *Geology*, *29*, 819–822.

Locke, A., P. Billingsley, and E. B. Mayo (1940), Sierra Nevada tectonic patterns, *Geol. Soc. Am. Bull.*, *51*, 513–540.

Lubetkin, L. K. C. (1988), Late Quaternary activity along the Lone Pine Fault, eastern California, *Geol. Soc. Am. Bull.*, *100*, 755–766.

Luyendyk, B. P. (1991), A model for Neogene crustal rotations, transtension, and transpression in southern California, *Geol. Soc. Am. Bull.*, *103*, 1528–1536.

Luyendyk, B. P., M. J. Kamerling, and R. Terres (1980), Geometric model for Neogene crustal rotations in southern California, *Geol. Soc. Am. Bull.*, *91*, 211–217.

Machette, M. N. (1978), Dating Quaternary faults in the southwestern United States by using buried calcic horizons, *J. Res. U. S. Geol. Surv.*, *6*, 369–381.

McGill, S., and T. K. Rockwell (1998), Ages of late Holocene earthquakes on the central Garlock Fault near El Paso Peaks, California, *J. Geophys. Res.*, *103*, 7265–7279.

McKee, E. H. (1968), Age and rate of movement of the northern part of the Death Valley-Furnace Creek fault zone, California, *Geol. Soc. Am. Bull.*, *79*, 509–512.

Minster, J. B., and T. H. Jordan (1987), Vector constraints on western U.S. deformation from space geodesy, neotectonics, and plate motions, *J. Geophys. Res.*, *92*, 4798–4804.

Moore, J. G., and C. A. Hopson (1961), The Independence Dike swarm in eastern California, *Am. J. Sci.*, *259*, 241–259.

Nicholson, C., L. Seeber, P. Williams, and L. R. Sykes (1986), Seismic evidence for conjugate slip and block rotation within the San Andreas fault system, southern California, *Tectonics*, *5*, 629–648.

Nicholson, C., C. C. Sorlien, T. Atwater, J. C. Crowell, and B. P. Luyendyk (1994), Microplate capture, rotation of the western Transverse Ranges, and initiation of the San Andreas transform as a low-angle fault system, *Geology*, *22*, 491–495.

Nielsen, R. L. (1965), Right-lateral strike-slip faulting in the Walker Lane, west-central Nevada, *Geol. Soc. Am. Bull.*, *76*, 1301–1308.

Nur, A., H. Ron, and O. Scott (1986), Fault mechanics and the kinematics of block rotations, *Geology*, *14*, 746–749.

Oldow, J. S. (1984), Evolution of a late Mesozoic back-arc fold and thrust belt, northwestern Great Basin, USA, *Tectonophysics*, *102*, 245–274.

Oldow, J. S. (1992), Late Cenozoic displacement partitioning in the northwestern Great Basin, in *Structure, Tectonics, and Mineralization of the Walker Lane*, edited by S. D. Craig, pp. 17–52, Geol. Soc. of Nev., Reno.

Oldow, J. S., and J. S. Dockery (1993), Geologic map of the Mina quadrangle, Nevada, 1:24,000, *Nev. Bur. Mines Geol. Field Stud. Map, 6*.

Oldow, J. S., and J. N. Meinwald (1992), Geologic map of the Bettles Well quadrangle, Nevada, Nev. Bur. of Mines and Geol., Reno.

Oldow, J. S., G. Kohler, and R. A. Donelick (1994), Late Cenozoic extensional transfer in the Walker Lane strike-slip belt, Nevada, *Geology*, *22*, 637–640.

Oldow, J. S., C. L. V. Aiken, J. L. Hare, H. G. Ferguson, and R. F. Hardyman (2001), Active displacement transfer and differential block motion within the Central Walker Lane, western Great Basin, *Geology*, *29*, 19–22.

Oswald, J. O., and S. G. Wesnousky (2002), Neotectonics and Quaternary geology of the Hunter Mountain fault zone and Saline Valley region, southeastern California, *Geomorphology*, *42*, 255–278.

Peltzer, G., F. Crampe, S. Hensley, and P. Rosen (2001), Transient strain accumulation and fault interaction in the Eastern California Shear Zone, *Geology*, *29*, 975–978.

Ramelli, A. R., J. W. Bell, C. M. dePolo, and J. C. Yount (1999), Large-magnitude, late Holocene earthquakes on the Genoa Fault, west-central Nevada and eastern California, *Bull. Seismol. Soc. Am.*, *89*, 1458–1472.

Reheis, M. C., and T. H. Dixon (1996), Kinematics of the Eastern California Shear Zone: Evidence for slip transfer from Owens and Saline Valley fault zones to Fish Lake Valley fault zone, *Geology*, *24*, 339–342.

Reheis, M. C., and E. H. McKee (1991), Late Cenozoic history of slip on the Fish Lake Valley fault zone, Nevada and California, *U.S. Geol. Surv. Open File Rep.*, *91-290*, 26–45.

Reheis, M. C., and T. L. Sawyer (1997), Late Cenozoic history and slip rates of the Fish Lake Valley, Emigrant Peak, and Deep Springs fault zone, Nevada

and California, *Geol. Soc. Am. Bull.*, *109*, 280–299.

Reheis, M. C., J. Slate, and T. L. Sawyer (1995), Geologic map of late Cenozoic deposits and faults in parts of the Mt. Barcroft, Piper Peak, and Soldier Pass 15′ quadrangles, Esmeralda County, Nevada, and Mono County, California, *U.S. Geol. Surv. Misc. Invest. Ser. Map, I-2464*, scale 1:24,000.

Reheis, M. C., A. M. Sarna-Wojcicki, R. L. Reynolds, C. A. Repenning, and M. D. Mifflen (2002), Pliocene to middle Pleistocene lakes in the western Great Basin: Ages and connections, in *Great Basin Aquatic Systems History*, edited by R. Hershler, D. Currey, and D. Madsen, *Smithson. Contrib. Earth Sci.*, *33*, 53–108.

Rogers, D. K. (1975), The Carson Lineament: Its influence on recent left-lateral faulting near Carson City, Nevada, *Geol. Soc. Am. Abstr. Programs.*, *7*, 1250.

Ron, H., R. Freund, and Z. Garfunkel (1984), Block rotation by strike-slip faulting: Structural and paleomagnetic evidence, *J. Geophys. Res.*, *89*, 6256–6270.

Ross, D. C. (1962), Correlation of granitic plutons across faulted Owens Valley, California, *U.S. Geol. Surv. Prof. Pap.*, *450-D*, D86–D88.

Sanders, C. O., and D. B. Slemmons (1979), Recent crustal movements in the central Sierra Nevada-Walker Lane region of California: Part III, The Olinghouse fault zone, *Tectonophysics*, *52*, 585–597.

Sanders, C. O., and D. B. Slemmons (1996), Geomorphic evidence for Holocene earthquakes in the Olinghouse fault zone, western Nevada, *Bull. Seismol. Soc. Am.*, *86*, 1784–1792.

Sarna-Wojcicki, A. M., and J. O. Davis (1991), Quaternary tephrochronology, in *Geology of North America*, vol. K2, *Quaternary Nonglacial Geology: Conterminous U. S.*, edited by R. B. Morrison, pp. 93–116, Geol. Soc. of Am., Boulder, Colo.

Sarna-Wojcicki, A. M., K. R. Lajoie, C. E. Meyer, D. P. Adam, and H. J. Rieck (1991), Tephrochronologic correlation of upper Neogene sediments along the Pacific margin, conterminous United States, in *Geology of North America*, vol. K-2, *Quaternary Nonglacial Geology: Conterminous U. S.*, edited by R. B. Morrison, pp. 117–140, Geol. Soc. of Am., Boulder, Colo.

Sarna-Wojcicki, A. M., et al. (2005), Tephra layers of Blind Spring valley and related upper Pliocene and Pleistocene tephra layers, California, Nevada and Utah: Isotopic ages, correlation, and magnetostratigraphy, *U.S. Geol. Surv. Open File Rep.*, *1701*, 69 pp.

Sauber, J. (1994), Geodetic slip rate for the eastern California shear zone and the recurrence time of Mojave Desert earthquakes, *Nature*, *367*, 264–266.

Sauber, J., W. Thatcher, and S. C. Solomon (1986), Geodetic measurements of deformation in the central Mojave Desert, California, *J. Geophys. Res.*, *91*, 12,661–12,674.

Savage, J. C., W. J. Gan, and J. L. Svarc (2001), Strain accumulation and rotation in the Eastern California Shear Zone, *J. Geophys. Res.*, *106*, 21,995–22,007.

Slemmons, D. B., D. Van Wormer, E. J. Bell, and M. L. Silberman (1979), Recent crustal movements in the Sierra Nevada-Walker Lane region of California-Nevada: Part I, rate and style of deformation, *Tectonophysics*, *52*, 561–570.

Smith, G. I. (1962), Large lateral displacement on Garlock Fault, California, as measured from offset dike swarm, *Am. Assoc. Pet. Geol. Bull.*, *46*, 85–104.

Speed, R. C. (1981), Preliminary geologic map of the Sodaville quadrangle, Mineral County, Nevada, *U.S. Geol. Surv. Misc. Field Stud. Map MF-1300*, scale 1:24,000.

Speed, R. C., and A. H. Cogbill (1979), Candelaria and other left-oblique slip faults of the Candelaria region, Nevada, *Geol. Soc. Am. Bull.*, *90*, I-149–I-163.

Stewart, J. H. (1978), Geologic map of Nevada, *U.S. Geol. Surv.*, scale 1:500,000.

Stewart, J. H. (1980), Geology of Nevada, *Nev. Bur. Mines Geol. Spec. Publ.*, *4*, 1–136.

Stewart, J. H. (1981), Geology of the Basalt quadrangle, Mineral County, Nevada, 1:24,000, *U.S. Geol. Surv. Open File Rep., 82-369*.

Stewart, J. H. (1984), Geologic map of the Teels Marsh quadrangle, Mineral County, Nevada, 1:24,000, *U.S. Geol. Surv. Open File Rep., 84-504*.

Stewart, J. H. (1985), East-trending dextral faults in the western Great Basin; an explanation for anomalous trends of pre-Cenozoic strata and Cenozoic faults, *Tectonics*, *4*, 547–564.

Stewart, J. H. (1988), Tectonics of the Walker Lane Belt, western Great Basin Mesozoic and Cenozoic deformation in a zone of shear, in *Metamorphism and Crustal Evolution of the Western U.S., Ruby Volume VII*, edited by W. G. Ernst, pp. 685–713, Prentice-Hall, Upper Saddle River, N. J.

Stewart, J. H., F. J. Kleinhampl, D. C. Johannesen, R. C. Speed, and J. C. Dohrenwend (1981), Geologic map of the Huntoon Valley quadrangle, Mineral County, Nevada and Mono County, California, *Geol. Surv. Open File Rep., 81-0274*, scale 1:62,500.

Stewart, J. H., J. E. Carlson, and D. C. Johannesen (1982), Geologic map of the Walker Lake 1° by 2° quadrangle, California and Nevada, *U.S. Geol. Surv. Misc. Field Stud. Map, MF-1382a*, scale 1:250,000.

Stewart, J. H., F. J. Kleinhampl, and D. C. Johannesen (1984), Geologic map of the Rattlesnake Flat quadrangle, Mineral County, Nevada, *U.S. Geol. Surv. Open File Rep., 84-506*, scale 1:24,000.

Stirling, M. W., S. G. Wesnousky, and K. Shimazaki (1996), Fault trace complexity, cumulative slip, and the shape of the magnitude-frequency distribution for strike-slip faults: A global survey, *Geophys. J. Int.*, *124*, 833–868.

Stockli, D. F., B. E. Surpless, T. A. Dumitru, and K. A. Farley (2002), Thermochronological constraints on the timing and magnitude of Miocene and Pliocene extension in the central Wassuk Range, western Nevada, *Tectonics*, *21*(4), 1028, doi:10.1029/2001TC001295.

Stuiver, M., and H. A. Polach (1977), Discussion: Reporting of ^{14}C data, *Radiocarbon*, *19*, 355–363.

Stuiver, M., and P. J. Reimer (1993), Extended ^{14}C database and revised CALIB radiocarbon calibration program, *Radiocarbon*, *35*, 215–230.

Thatcher, W., G. R. Foulger, B. R. Julian, J. L. Svarc, E. Quilty, and G. W. Bawden (1999), Present-day deformation across the Basin and Range province, western United States, *Science*, *283*, 1714–1717.

Toppozada, T. R., C. R. Real, and D. L. Parke (1981), Preparation of isoseismal maps and summaries of reported effects for pre-1990 California earthquakes, *Calif. Div. Mines Geol. Open File Rep., 81-11*, 1–182.

Unruh, J., J. Humphrey, and A. Barron (2003), Transtensional model for the Sierra Nevada frontal fault system, eastern California, *Geology*, *31*, 327–330.

Vedder, J. G., and R. E. Wallace (1970), Map showing recently active breaks along the San Andreas and related faults between Cholame Valley and Tejon Pass, California, U.S. Geol. Surv., Reston, Va.

Wahrhaftig, C., and R. P. Sharp (1965), Sonora Pass Junction to Bloody Canyon, in *INQUA 7th Congress*: *Guidebook for Field Conference I - Northern Great Basin and California*, pp. 71–84, Int. Union for Quat. Res., Dublin, Ireland.

Wallace, R. E. (1977), Profiles and ages of young fault scarps, north-central Nevada, *Geol. Soc. Am. Bull.*, *88*, 1267–1281.

Wallace, R. E. (1978a), Geometry and rates of change of fault-generated range fronts, north-central Nevada, *J. Res. U.S. Geol. Surv.*, *6*, 637–650.

Wallace, R. E. (1978b), Patterns of faulting and seismic gaps in the Great Basin Province, in *Proceedings of Conference VI, Methodology for Identifying Seismic Gaps and Soon-to-Break Gaps*, *U.S. Geol. Surv. Open File Rep., 78-943*, 857–868.

Wallace, R. E. (1984), Patterns and timing of late Quaternary faulting in the Great Basin Province and relation to some regional tectonic features, *J. Geophys. Res.*, *89*, 5769–6763.

Wallace, R. E. (1990), Geomorphic expression, in *The San Andreas Fault System*, edited by R. E. Wallace, pp. 15–60, U.S. Geol. Surv., Reston, Va.

Wesnousky, S. G. (1988), Seismological and structural evolution of strike-slip faults, *Nature*, *335*, 340–343.

Wesnousky, S. G. (2005), The San Andreas and Walker Lane fault systems, western North America: Transpression, transtension, cumulative slip and the structural evolution of a major transform plate boundary, *J. Struct. Geol.*, in press.

Wesnousky, S. G., and C. H. Jones (1994), Oblique slip, slip partitioning, spatial and temporal changes in the regional stress field, and the relative strength of active faults in the Basin and Range, western United States, *Geology*, *22*, 1031–1034.

Wetterauer, R. H. (1977), The Mina deflection: A new interpretation based on the history of the Lower Jurassic Dunlap formation, western Nevada, Ph.D. thesis, 155 pp., Northwestern Univ., Evanston, Ill.

Wilcox, R. E., T. P. Harding, and D. R. Seely (1973), Basic wrench tectonics, *Am. Assoc. Pet. Geol. Bull.*, *57*, 74–96.

Wills, C. J., and G. Borchardt (1993), Holocene slip rate and earthquake recurrence on the Honey Lake fault zone, northeastern California, *Geology*, *21*, 853–856.

Zhang, P., M. Ellis, D. B. Slemmons, and F. Mao (1990), Right-lateral displacements and the Holocene slip rate associated with prehistoric earthquakes along the southern Panamint Valley fault zone: Implications for southern Basin and Range tectonics and coastal California deformation, *J. Geophys. Res.*, *95*, 4857–4872.

S. G. Wesnousky, Center for Neotectonic Studies, University of Nevada, Mail Stop 169, Reno, NV 89557, USA. (stevew@seismo.unr.edu)